

$\pi^+ - \pi^0$ mass difference and S parameter in the large N_f QCD*

Masayasu HARADA^a, Masafumi KURACHI^b, and Koichi YAMAWAKI^a,

^a*Department of Physics, Nagoya University
Nagoya 464-8602, Japan*

^b*Department of Physics, Tohoku University
Sendai 980-8578, Japan*

and

*C.N. Yang Institute for Theoretical Physics, State University of New York,
Stony Brook, NY 11794, U.S.A.*[†]

Abstract

In the framework of the Schwinger-Dyson equation and the Bethe-Salpeter equation in the improved ladder approximation, we calculate the S parameter and an analogue of the $\pi^+ - \pi^0$ mass difference $\Delta m_\pi^2 \equiv m_{\pi^+}^2 - m_{\pi^0}^2$ as well as the NG boson decay constant f_π on the same footing in the large N_f QCD, through the difference between the vector current correlator Π_{VV} and the axial-vector current correlator Π_{AA} . Approaching the chiral phase transition point $\alpha_* \rightarrow \alpha_{\text{cr}} (= \pi/4)$ from the broken phase, where α_* is the gauge coupling on the infrared fixed point, Δm_π^2 as well as f_π^2 goes to zero with the essential-singularity scaling (Miransky scaling), while the ratio indicates a blowing up enhancement reflecting the characteristic behavior of the large N_f QCD as a walking theory which is expected to scale as $\Delta m_\pi^2 / f_\pi^2 \sim (\alpha_* / \alpha_{\text{cr}} - 1)^{-1/2}$. On the other hand, the S parameter takes values somewhat smaller than that of the real-life QCD and indicates slightly decreasing tendency as we approach the phase transition point.

*A preliminary report [1] was given at the 2004 International Workshop on Dynamical Symmetry Breaking (DSB04), December 21-22, 2004, Nagoya University, Nagoya.

[†]Present address

1 Introduction

The electroweak symmetry breaking in the standard model (SM) is well described by introducing the Higgs boson. However, the Higgs sector in the SM cannot *explain* the origin of the electroweak symmetry breaking, which means the SM cannot explain the origin of mass. Moreover, the mass of the Higgs particle has to be fine tuned since it receives quantum correction which is proportional to the square of the cutoff scale Λ . These facts naturally lead us to the idea that the Higgs sector in the SM is nothing but an low energy effective theory of some underlying theory. To consider the existence of a new strong dynamics is one example of this idea.

The “large N_f QCD”, a jargon of the $SU(3)$ gauge theory with a large number of massless fermions ($N_f \lesssim \frac{11}{2}N_c$) [2, 3, 4, 5, 6, 7, 8, 9, 10], is one of the candidates for such a strong dynamics like the technicolor [11, 12] which breaks the electroweak symmetry. Actually, it has interesting features:

- A dynamical model for the walking/conformal (scale-invariant) technicolor
It was observed [2] that QCD has an infrared (IR) fixed point $\alpha = \alpha_*$ for a large number of massless fermions ($N_f \lesssim \frac{11}{2}N_c$) at the two-loop beta function. It was regarded [3, 4] as a good example of the walking technicolor [13], because the running gauge coupling near the infrared fixed point is almost constant, $\alpha(Q^2) \simeq \alpha_*$, namely “walking” for a wide range of the momenta Q .

Moreover, it was found [3] through the improved ladder Schwinger-Dyson (SD) equation that chiral symmetry restoration takes place for certain N_f such that the IR fixed point becomes less than the critical coupling which is determined by the SD equation, namely $N_f^{\text{crit}} < N_f < \frac{11}{2}N_c$, where $N_f^{\text{crit}} \simeq 4N_c (= 12 \text{ for } N_c = 3)$. In Ref. [4] this chiral phase transition at N_f^{crit} was further identified with the “conformal phase transition” which was characterized by the essential singularity scaling (Miransky scaling). Moreover, the chiral restoration in large N_f QCD was also observed in lattice simulations [5] and by other various methods such as the dispersion relation [6], instanton calculus [7], effective field theoretical approach [8], renormalization group flow equations [10], perturbative calculus [14], etc., although the value of N_f^{crit} is raging from $N_f^{\text{crit}} \sim 5$ to $N_f^{\text{crit}} \sim 12$ ($N_c = 3$) depending on the approaches.

- A model for the electroweak baryogenesis
The electroweak baryogenesis [15] (for a review see, e.g., Ref.[16]) is an attractive scenario but has serious difficulties: 1) lack of mechanism to produce the first order phase transition consistently with the present experimental lower bound of the Higgs boson mass and 2) smallness of the baryon asymmetry if the CP violation is solely due to the KM phase in the Standard Model. The large N_f QCD when applied to the technicolor has new ingredients to solve these problems: It is widely believed [17] that QCD phase transition is the first order when the number of massless flavors exceeds 3 and, we expect, so is the chiral phase transition in the large N_f QCD. Moreover, it was argued [18] that the technicolor may have extra sources of the CP violation other than the KM phase and supply enough amount of CP violation needed for the baryogenesis.

Besides application to the technicolor, much attention has been paid to the property of the phase transition not just the existence of the chiral phase transition in the large N_f QCD. Especially, it is interesting to ask what are the light degrees of freedom near the phase transition point in the large N_f QCD: For example, in the manifestation of the chiral symmetry restoration á la linear sigma model (Ginzburg-Landau type effective theory), the scalar bound state becomes a chiral partner of the pseudoscalar bound state and becomes massless at the phase transition point when approached both from the broken and the symmetric phases. However, it was emphasized from the viewpoint of the conformal phase transition [4] that the Ginzburg-Landau type effective theory breaks down in the approach of the improved ladder SD equation, signaled by the absence of massless scalar bound state in the symmetric phase. Quite recently, such a peculiarity of the phase transition was also observed based on the renormalization-group analysis [10]. Besides, from the viewpoint of the conformal phase transition, it is natural to suppose that all the existing bound states become massless near the phase transition point when approached from the broken phase (see Ref. [19]). On the other hand, in the vector manifestation [9] obtained by the effective field theoretical approach based on the hidden local symmetry theory [20], it is the vector bound state which becomes massless as a chiral partner of the pseudoscalar bound state. It remains unclear at this moment whether or not the vector manifestation contradicts the conformal phase transition.

In Ref. [21], in the framework of the SD and the homogeneous Bethe-Salpeter (HBS) equations (see [22] for a review), we studied which types of the light bound states actually exist near the phase transition point, and investigated the critical behavior of their masses directly from QCD. We found that approaching the chiral phase transition point from the broken phase, the scalar, vector, and axial-vector meson masses vanish to zero with the same scaling behavior, all degenerate with the massless pseudoscalar meson.

In this paper, we further investigate the properties of the chiral phase transition in the large N_f QCD through the critical behavior of the S parameter and the “ $\pi^+ - \pi^0$ mass difference $\Delta m_\pi^2 \equiv m_{\pi^+}^2 - m_{\pi^0}^2$ ”, by extending our previous work [23] on the S parameter and Δm_π^2 done for the real-life QCD with $N_c = N_f = 3$. They are interesting quantities when we apply the dynamical symmetry breaking scenario based on the large N_f QCD for the model buildings beyond the SM like the walking technicolor, UV completions (underlying theories) for the little Higgs models [24] and the Higgsless models [25], etc.

Actually, there are strong constraints on the electroweak S parameter [26] from electroweak precision tests, it is quite important to estimate the S parameter theoretically when we consider the technicolor-like scenario. Estimation of masses of pseudo NG bosons is also important to check that the model is consistent with the fact that such a pseudo NG bosons have not been discovered so far. Then, it is desirable to estimate the S parameter and Δm_π^2 reliably.

Several attempts to estimate the parameter \hat{S} , which is the contribution to the S parameter from one weak fermionic doublet, for the walking technicolor theories and the large N_f QCD have been made so far by using several methods [27, 28]. However, it is difficult to estimate the accuracy of these calculation (see, for example, Ref. [29]).

What makes it difficult to estimate the S parameter is its strong dependence on the nonperturbative dynamics of the low momentum region. Then it is quite important to calculate the S parameter by using the nonperturbative method in a way to directly deal the fermions and the gauge bosons as the fundamental degrees of freedom.

As such, in the previous work [23], we calculated the S parameter and Δm_π^2 in the real-life ($N_f = 3$) QCD through the difference between the vector current correlator Π_{VV} and the axial-vector current correlator Π_{AA} . $\Pi_{VV} - \Pi_{AA}$ were calculated in the framework of the SD equation and the inhomogeneous Bethe-Salpeter (IBS) equation in the improved ladder approximation. It was stressed that these physical quantities are calculated by using the correlators *in the space-like region*, so that no analytic continuation is needed. The results in Ref. [23] shows that both the S parameter and Δm_π^2 can be fit to the experimental values at the same time. By fitting to the calculated data using the pole saturated form of $\Pi_{VV} - \Pi_{AA}$, we also derived masses and decay constants of ρ meson and A_1 meson, which we found are consistent with the experiments. This is quite encouraging to extend our method to the large N_f QCD.

In extending the previous method to the large N_f QCD, let us consider the situation that $SU(N_f)_L \otimes SU(N_f)_R$ chiral symmetry is explicitly broken by the $U(1)$ gauge symmetry. We take the generator of this $U(1)$ gauge symmetry as

$$Q = \begin{pmatrix} 2/3 & & & \\ & -1/3 & & \\ & & \ddots & \\ & & & \ddots \end{pmatrix}. \quad (1.1)$$

Then, we calculate the mass of the pseudo Nambu-Goldstone (NG) boson which is associated with the following generator:[30]

$$T_{pNGB} = \begin{pmatrix} 0 & 1 & 0 & \cdots \\ 0 & 0 & 0 & \\ 0 & 0 & 0 & \\ \vdots & & & \ddots \end{pmatrix}. \quad (1.2)$$

In the case of the real-life QCD, the above pseudo NG boson corresponds to the π^+ meson, and its (squared) mass caused by the $U(1)$ electro-magnetic gauge interaction corresponds to the $\pi^+ - \pi^0$ mass difference $\Delta m_\pi^2 \equiv m_{\pi^+}^2 - m_{\pi^0}^2$. Then, throughout this paper, we call the squared mass of the above pseudo NG boson “ Δm_π^2 ” even in the case of $N_f \neq 3$.

We then calculate \hat{S} and Δm_π^2 as well as f_π at the same time. We find that as we approach the critical point both Δm_π^2 and f_π^2 vanish in the essential singularity scaling (Miransky-type scaling), $\sim \exp\left(-2q/\sqrt{\alpha_*/\alpha_{\text{cr}} - 1}\right)$, ($q = \text{const.}$) with the ratio $\Delta m_\pi^2/f_\pi^2$ being *much enhanced* compared with that of the real-life QCD and having a blowing up tendency reflecting the inverse square root scaling, $\Delta m_\pi^2/f_\pi^2 \sim (\alpha_*/\alpha_{\text{cr}} - 1)^{-1/2}$, which is characteristic to the walking gauge coupling with large anomalous dimension $\gamma_m \simeq 1$ of the large N_f QCD. In fact the integral for the $\Delta m_\pi^2/f_\pi^2$ is expected to be logarithmically divergent for the walking theory, $\sim \ln(\Lambda^2/\Lambda_\chi^2)$, if

the walking behavior $\Pi_{VV} - \Pi_{AA} \sim 1/Q^2$ is operative for $\Lambda_\chi < Q^2 < \Lambda^2$, where Λ is the (two-loop) scale parameter of the large N_f QCD like Λ_{QCD} in the real-life QCD, and $\Lambda_\chi \simeq 4\pi f_\pi \sim \Lambda \exp\left(-q/\sqrt{\alpha_*/\alpha_{\text{cr}}} - 1\right)$. In the actual numerical calculations we used an artificial cutoff Λ_{Num} which is defined for the sake of numerical calculations as $\Pi_{VV} - \Pi_{AA}|_{Q^2=\Lambda_{\text{Num}}^2} = \frac{1}{50} [\Pi_{VV} - \Pi_{AA}]|_{Q^2=0}$ (we will later include contributions from $\Lambda_{\text{Num}}^2 < Q^2 < \Lambda^2$, based on the analytical considerations on the walking theory). Up to this limitation the numerical result is already enhanced up till $\Delta m_\pi^2/f_\pi^2 \simeq 0.6$, about four times larger than that obtained in the same method for the real-life QCD, $\Delta m_\pi^2/f_\pi^2 \simeq 0.123$ [23] (experimental value: $\Delta m_\pi^2/f_\pi^2 = 0.148 \pm 0.001$), even though our calculation is still away from the critical point for the reason of the computation ability. (If we include contributions from $\Lambda_{\text{Num}}^2 < Q^2 < \Lambda^2$, the enhancement is more dramatic).

This implies a *large enhancement factor* for the pseudo NG boson mass in the walking/conformal (scale-invariant) technicolor [13].¹ If it is applied to the popular one-family model (Farhi-Susskind model) [12], the mass² of the P^\pm (and also of the colored pseudo NG bosons) as a scale-up of Δm_π^2 essentially irrelevant to the ETC interactions, will be enhanced also by a large anomalous dimension $\gamma_m \simeq 1$ by a factor four (to nine): The mass of P^\pm will be boosted to typically more than 200(–300)GeV mass range instead of 100GeV the value in a simple scale up of QCD. If we consider the model which is closer to the critical point, the enhancement factor should be more dramatic due to the inverse square root scaling mentioned above.

On the other hand, the values of \hat{S} in our calculations are somewhat smaller $\hat{S} = 0.25 - 0.30$ than that obtained in the same method for the real-life QCD ($N_c = N_f = 3$), $S = \hat{S} \simeq 0.33$ [23] (experimental value: $S = 0.32 \pm 0.04$), and indicate a tendency to decrease slightly as we approach to the critical point. Although it is still larger than the simple one-loop result $\hat{S} = \frac{N_c}{6\pi} = 0.16$ ($N_c = 3$), it could be suggestive for a further decreasing towards the critical point. It would motivate further study in the points closer to the critical point to see whether or not technicolor model based on the large N_f QCD makes S consistent with the present experimental bound $S < 0.1$.

The calculation in this paper turns out to be the first example which estimates the S parameter and Δm_π^2 in the large N_f QCD as a model of walking technicolor by directly solving its dynamics².

This paper is organized as follows. In the next section, we briefly review the large N_f QCD. In section 3, we introduce sum rules: The DMO sum rule or the zeroth Weinberg sum rule for the parameter \hat{S} , the first Weinberg sum rule for f_π^2 , and the DGMLY sum rule or the third Weinberg sum rule for Δm_π^2 . We then rewrite them in terms of the current correlators $\Pi_{VV} - \Pi_{AA}$. In section 4, we show how the current correlators are obtained from the BS amplitudes calculated from the IBS equation in the space-like region. In section 5, we introduce the IBS equation. In section 6, we show the results of numerical calculation for critical behaviors of f_π , Δm_π^2 and \hat{S} .

¹A similar enhancement of pseudo NG boson mass in the walking technicolor (other than the large N_f QCD) was also observed by a numerical study in a different approach [31].

²In Ref. [32], the S parameter in the walking technicolor theory was calculated by using the BS equation. However, the S parameter in the large N_f QCD was not calculated.

Section 7 is devoted to conclusion and discussions.

2 Large N_f QCD

In QCD with N_f flavors of massless quarks, the renormalization group equation (RGE) for the running coupling $\alpha(\mu)$ ($= \frac{\bar{g}^2(\mu)}{4\pi}$) in the two-loop approximation is given by

$$\mu \frac{d}{d\mu} \alpha(\mu) = -b\alpha^2(\mu) - c\alpha^3(\mu), \quad (2.1)$$

where

$$b = \frac{1}{6\pi} (11N_c - 2N_f) \quad , \quad c = \frac{1}{24\pi^2} \left(34N_c^2 - 10N_cN_f - 3\frac{N_c^2 - 1}{N_c}N_f \right) . \quad (2.2)$$

From the above beta function we can easily see that, when $b > 0$ and $c < 0$, i.e., N_f takes a value in the range of $N_f^* < N_f < \frac{11}{2}N_c$ ($N_f^* \simeq 8.05$ for $N_c = 3$), the theory is asymptotically free and the beta function has a zero, corresponding to an infrared stable fixed point [2, 3], at

$$\alpha_* = -\frac{b}{c} . \quad (2.3)$$

Existence of the infrared fixed point implies that the running coupling takes a finite value even in the low energy region. Actually, the solution of the two loop RGE in Eq. (2.1) can be explicitly written [33, 34] in all the energy region as

$$\alpha(\mu) = \alpha_* \left[W(\mu^{b\alpha_*}/e\Lambda^{b\alpha_*}) + 1 \right]^{-1}, \quad (2.4)$$

where $W(x) = F^{-1}(x)$ with $F(x) = xe^x$ is the Lambert W function, and Λ is a renormalization group invariant scale defined by [3]

$$\Lambda \equiv \mu \exp \left[-\frac{1}{b\alpha_*} \log \left(\frac{\alpha_* - \alpha(\mu)}{\alpha(\mu)} \right) - \frac{1}{b\alpha(\mu)} \right]. \quad (2.5)$$

We note that, in the present analysis, we fix Λ to compare the theories with a different number of flavors, and that we have no adjustable parameters in the running coupling in Eq. (2.4), accordingly.³ We show an example of $\alpha(\mu)$ for $N_f = 9$ in Fig. 1. The fact that the running coupling is expressed by a certain function as in Eq. (2.4) implies that, in the case of the large N_f QCD, *we do not need to introduce any infrared regularizations* such as those adopted in Ref. [23], or in Refs. [35] for studying real-life QCD with small N_f in which the infrared regularization parameter must be chosen in

³Note that we do not have to specify the value of Λ , since in this paper we calculate only dimensionless quantities, S parameter and $\Delta m_\pi^2/f_\pi^2$, which are independent of the actual value of Λ in unit of, say GeV. When we apply the dynamics to the model building for the electroweak symmetry breaking, we should specify the value of f_π (of order of the weak scale 250 GeV but actually model-dependent) and then determine the scale of Λ as a function of $N_c (= 3)$ and N_f as well as f_π (See Fig.3).

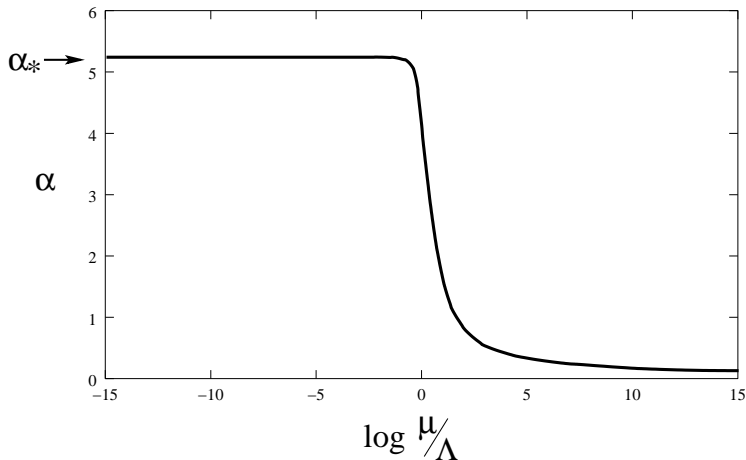


Figure 1: Two-loop running coupling of the large N_f QCD for $N_f = 9$.

such a way that the running coupling in the infrared region becomes larger than the critical value $\alpha_{\text{cr}} = \pi/4$ for realizing the dynamical chiral symmetry breaking. The running coupling in the large N_f QCD takes a certain value in the infrared region for given N_f , so that we can definitely determine, within the framework of the SD equation, whether or not the dynamical chiral symmetry breaking of $SU(N_f)_L \times SU(N_f)_R \rightarrow SU(N_f)_V$ is realized. Actually, the value of α_* decreases monotonically with increasing N_f , and the chiral symmetry restores when N_f becomes large enough. In Refs. [3], it was shown that the phase transition occurs at $N_f^{\text{crit}} \simeq 11.9$ for $N_c = 3$ (corresponding to $\alpha_* = \alpha_{\text{cr}} = \pi/4$). However, the value of N_f^{crit} itself should not be taken seriously, since $\alpha_{\text{cr}} = \pi/4$ to be equated to α_* is already so large as to invalidate the perturbation which determined the value of α_* . There is also some ambiguity of the ladder approximation which determined the value $\alpha_{\text{cr}} = \pi/4$ itself. In fact lattice simulations [5] suggest smaller value $6 < N_f^{\text{crit}} < 7$ and other approaches also suggest different values [6, 7, 8, 10].

3 Expressions of f_π , \hat{S} and Δm_π^2 in terms of current correlators

In this section we introduce sum rules for expressing the order parameter f_π , the parameter \hat{S} which is the contribution to the S parameter from one weak fermionic doublet, and the square mass of the pseudo NG Δm_π^2 in terms of $\Pi_{VV} - \Pi_{AA}$ in the space-like momentum region.

Let us begin with introducing the vector and the axial-vector currents as

$$\begin{aligned} V_\mu^a(x) &= \bar{\psi}(x) T^a \gamma_\mu \psi(x), \\ A_\mu^a(x) &= \bar{\psi}(x) T^a \gamma_\mu \gamma_5 \psi(x), \end{aligned} \quad (3.1)$$

where T^a ($a = 1, 2, \dots, N_f^2 - 1$) is the generator of $SU(N_f)$ normalized as $\text{tr}(T^a T^b) = \frac{1}{2} \delta^{ab}$. As we discussed in the previous section, for $N_f < N_f^{\text{crit}}$ there occurs the spon-

taneous symmetry breaking of $SU(N_f)_L \times SU(N_f)_R \rightarrow SU(N_f)_V$. As a result, the massless NG boson π appears, whose decay constant f_π is defined as

$$\langle 0|A_\mu^a(0)|\pi^b(q)\rangle = iq_\mu f_\pi \delta^{ab}, \quad (3.2)$$

where $a, b = 1, 2, \dots, N_f^2 - 1$. As is well-known as the first Weinberg sum rule [36], the above decay constant is related the difference of the vector current correlator Π_{VV} and the axial-vector current correlator Π_{AA} as

$$f_\pi^2 = \Pi_{VV}(0) - \Pi_{AA}(0), \quad (3.3)$$

where the correlators are defined from the currents in Eq. (3.1) as

$$\delta^{ab} \left(\frac{q_\mu q_\nu}{q^2} - g_{\mu\nu} \right) \Pi_{JJ}(q^2) = i \int d^4x e^{iqx} \langle 0|T J_\mu^a(x) J_\nu^b(0)|0\rangle, \quad (3.4)$$

$$(J_\mu^a(x) = V_\mu^a(x), A_\mu^a(x)).$$

When the large N_f QCD is considered as the underlying theory for describing the Higgs sector of the standard model as in the technicolor-like scenario [11, 12], it is important to study the S parameter [26] which gets a strong constraint from the electroweak precision tests [37]. Since entire contributions to the S parameter depend on the detail of the model structure, we concentrate on calculating the contribution from one $SU(2)_L$ doublet with the hypercharge $Y = 1/6$ and two singlets with $Y = 2/3$ and $Y = -1/3$. This parameter \hat{S} is related to the above correlators as

$$\hat{S} = -4\pi \frac{d}{dQ^2} \left[\Pi_{VV}(Q^2) - \Pi_{AA}(Q^2) \right] \Big|_{Q^2=0}, \quad (3.5)$$

which is nothing but the DMO sum rule [38] or often called the ‘‘zeroth Weinberg sum rule’’.

Mass of the pseudo NG boson is also an important quantity in the technicolor-like scenario. In the present analysis, we consider the situation that $SU(N_f)_L \otimes SU(N_f)_R$ chiral symmetry is explicitly broken by the $U(1)$ gauge symmetry, the generator of which is given as in Eq. (1.1), and calculate the the mass of the pseudo NG boson associated with the generator given in Eq. (1.2). The squared mass of the above pseudo NG boson Δm_π^2 is related to the above correlators as [39]

$$\Delta m_\pi^2 = \frac{3\alpha_{em}}{4\pi f_\pi^2} \int_0^\infty dQ^2 \left[\Pi_{VV}(Q^2) - \Pi_{AA}(Q^2) \right]. \quad (3.6)$$

where $\alpha_{em}(= \frac{e^2}{4\pi} = \frac{1}{137})$. Equation (3.6) was first derived by Das et al. [40] in the form written in terms of the spectral function instead of the current correlators and may be called the DGMLY sum rule or the ‘‘third Weinberg sum rule’’.

As was studied in, e.g., Ref. [41], Δm_π^2 is interesting quantity to study because it is related to the structure of the vacuum. When we switch off the above gauge interaction, we have $N_f^2 - 1$ massless NG bosons associated with the spontaneous breaking of $SU(N_f)_L \otimes SU(N_f)_R$ chiral symmetry down to $SU(N_f)_V$ symmetry. The

existence of the gauge interaction explicitly breaks the $SU(N_f)_L \otimes SU(N_f)_R$ chiral symmetry, which makes some of NG bosons (say π^+) be massive while others (say π^0) remain massless. The interesting point here is whether Δm_π^2 becomes positive or negative, which is called “vacuum alignment problem” [41]. Negative Δm_π^2 means that fluctuation of π^+ field around $\langle \pi^+ \rangle = 0$ is unstable and the vacuum with $\langle \pi^+ \rangle = 0$ is not a true vacuum. If this is the case, π^+ has non-zero vacuum expectation value and $U(1)$ gauge symmetry is broken. In the case of the real-life ($N_f = 3$) QCD, we have shown [23] that positive Δm_π^2 is successfully reproduced in the framework of the SD equation and the IBS equation with the improved ladder approximation. In our best knowledge, however, no one has explicitly shown whether positive Δm_π^2 is also realized in the case of the large N_f QCD, especially near the critical point, so our calculation is the first one which explicitly investigates the stability of the vacuum in the large N_f QCD.

4 Current correlators from BS amplitudes

In the previous section we have written down the sum rules for f_π , \hat{S} and Δm_π^2 in terms of the current correlators. In this section, we show how the current correlators are obtained from BS amplitudes which will be calculated from the IBS equation.

For deriving several properties of hadrons as boundstates, we often need to perform calculations in the time-like momentum region. However, it is difficult to solve the BS equation and the SD equation in the time-like region since we have to carry out the analytic continuation of the running coupling from the space-like region to the time-like region.⁴ In the present analysis, on the other hand, we need the BS amplitude only in the space-like region in order to calculate the current correlators appearing in the sum rules for Δm_π^2 , f_π and the QCD S parameter.

Now, the BS amplitudes $\chi^{(J)}$ ($J = V, A$) are defined in terms of the three-point vertex function as follows:

$$\delta_i^j (T^a)_{f'}^{f'} \int \frac{d^4 p}{(2\pi)^4} e^{-ipr} \chi_{\alpha\beta}^{(J)}(p; q, \epsilon) = \epsilon^\mu \int d^4 x e^{iqx} \langle 0 | T \psi_{\alpha if}(r/2) \bar{\psi}_{j' f'}^{j'}(-r/2) J_\mu^a(x) | 0 \rangle, \quad (4.1)$$

where q^μ is the total momentum of the fermion and the anti-fermion, and p^μ is the relative one. ϵ^μ is the polarization vector defined by $\epsilon \cdot q = 0$, $\epsilon \cdot \epsilon = -1$, and (f, f') , (i, j) , (α, β) are flavor, color and spinor indices, respectively. Closing the fermion legs of the above three-point vertex function and taking the limit $r \rightarrow 0$, we

⁴In general, one-loop running coupling of QCD is not analytic, so that several models for running coupling are introduced to solve the SD and BS equations in the time-like region. On the other hand, the running coupling at two-loop level becomes fully analytic near the phase transition point in the large N_f QCD. In Ref. [21], we approximated the analytic running coupling by a simple function $\frac{\bar{g}^2(x+y)}{4\pi} = \alpha_* \theta(\Lambda^2 - (x+y))$, and studied the critical behaviors of f_π as well as masses and decay constants of scalar, vector, and axial-vector mesons. We note that, in the present analysis, we do not use the approximate form, but use the fully analytic two-loop running coupling.

can express the current correlator in terms of the BS amplitude as follows:

$$\Pi_{JJ}(q^2) = \frac{1}{3} \sum_{\epsilon} \int \frac{d^4 p}{i(2\pi)^4} \frac{N_c}{2} \text{tr} \left[(\epsilon \cdot G^{(J)}) \chi^{(J)}(p; q, \epsilon) \right] \quad (4.2)$$

where

$$G_{\mu}^{(V)} = \gamma_{\mu}, \quad G_{\mu}^{(A)} = \gamma_{\mu} \gamma_5, \quad (4.3)$$

and $N_c = 3$ is the number of colors. In the above expression we averaged over the polarizations so that $\Pi_{JJ}(q^2)$ does not depend on the polarization.

We expand the BS amplitude $\chi_{\alpha\beta}^{(J)}(p; q, \epsilon)$ in terms of the bispinor bases $\Gamma_i^{(J)}$ and the invariant amplitudes $\chi_i^{(J)}$ as

$$\left[\chi^{(J)}(p; q, \epsilon) \right]_{\alpha\beta} = \sum_{i=1}^8 \left[\Gamma_i^{(J)}(p; \hat{q}, \epsilon) \right]_{\alpha\beta} \chi_i^{(J)}(p; q), \quad (4.4)$$

where $\hat{q}_{\mu} = q_{\mu}/\sqrt{Q^2}$ with $Q^2 = -q^2$. The bispinor bases can be chosen in a way that they have the same properties of spin, parity and charge conjugation as the corresponding current $J_{\mu}^a(x)$ has. We adopt the following bispinor bases for the vector vertex:

$$\begin{aligned} \Gamma_1^{(V)} &= \not{\epsilon}, \quad \Gamma_2^{(V)} = \frac{1}{2}[\not{\epsilon}, \not{p}](p \cdot \hat{q}), \quad \Gamma_3^{(V)} = \frac{1}{2}[\not{\epsilon}, \not{\hat{q}}], \quad \Gamma_4^{(V)} = \frac{1}{3!}[\not{\epsilon}, \not{p}, \not{\hat{q}}] \\ \Gamma_5^{(V)} &= (\epsilon \cdot p), \quad \Gamma_6^{(V)} = \not{p}(\epsilon \cdot p), \quad \Gamma_7^{(V)} = \not{\hat{q}}(p \cdot \hat{q})(\epsilon \cdot p), \quad \Gamma_8^{(V)} = \frac{1}{2}[\not{p}, \not{\hat{q}}](\epsilon \cdot p), \end{aligned} \quad (4.5)$$

where $[a, b, c] \equiv a[b, c] + b[c, a] + c[a, b]$. For the axial-vector vertex we use

$$\begin{aligned} \Gamma_1^{(A)} &= \not{\epsilon} \gamma_5, \quad \Gamma_2^{(A)} = \frac{1}{2}[\not{\epsilon}, \not{p}]\gamma_5, \quad \Gamma_3^{(A)} = \frac{1}{2}[\not{\epsilon}, \not{\hat{q}}] (p \cdot \hat{q}) \gamma_5, \\ \Gamma_4^{(A)} &= \frac{1}{3!}[\not{\epsilon}, \not{p}, \not{\hat{q}}] \gamma_5, \quad \Gamma_5^{(A)} = (\epsilon \cdot p) (p \cdot \hat{q}) \gamma_5, \quad \Gamma_6^{(A)} = \not{p}(\epsilon \cdot p) \gamma_5, \\ \Gamma_7^{(A)} &= \not{\hat{q}} (\epsilon \cdot p) (p \cdot \hat{q}) \gamma_5, \quad \Gamma_8^{(A)} = \frac{1}{2}[\not{p}, \not{\hat{q}}](\epsilon \cdot p) (p \cdot \hat{q}) \gamma_5. \end{aligned} \quad (4.6)$$

From the above choice of the bases, we can easily show that all the invariant amplitudes $\chi_i^{(J)}$ are the even functions of $(p \cdot \hat{q})$ using the charge conjugation property of the current.

In the present analysis we fix the frame of reference in such a way that only the zero component of the total momentum q^{μ} becomes non-zero. Furthermore, we study the case where q^{μ} is in the space-like region. Then, it is convenient to parameterize the total momentum q^{μ} as

$$q^{\mu} = (iQ, 0, 0, 0). \quad (4.7)$$

For the relative momentum p^{μ} , we perform the Wick rotation, and parameterize it by the real variables u and x as

$$p \cdot q = -Q u, \quad p^2 = -u^2 - x^2. \quad (4.8)$$

Consequently, the invariant amplitudes $\chi_i^{(J)}$ become functions in u and x :

$$\chi_i^{(J)} = \chi_i^{(J)}(u, x; Q). \quad (4.9)$$

From the charge conjugation properties for the BS amplitude $\chi^{(J)}$ and the bispinor bases defined above, the invariant amplitudes $\chi_i^{(J)}(u, x)$ are shown to satisfy

$$\chi_i^{(J)}(u, x; Q) = \chi_i^{(J)}(-u, x; Q). \quad (4.10)$$

Using this property of the invariant amplitudes, we rewrite Eq. (4.2) as

$$\Pi_{VV}(Q^2) = \frac{N_c}{\pi^3} \int_0^\infty du \int_0^\infty dx x^2 \left[-\chi_1^{(V)}(u, x; Q) + \frac{x^2}{3} \chi_6^{(V)}(u, x; Q) \right], \quad (4.11)$$

$$\Pi_{AA}(Q^2) = \frac{N_c}{\pi^3} \int_0^\infty du \int_0^\infty dx x^2 \left[\chi_1^{(A)}(u, x; Q) - \frac{x^2}{3} \chi_6^{(A)}(u, x; Q) \right]. \quad (4.12)$$

Here, we used the expanded form of the BS amplitude shown in Eq. (4.4) and carried out the three dimensional angle integration.

From Eqs. (4.11) and (4.12), the quantity $\Pi_{VV} - \Pi_{AA}$ is expressed as

$$\begin{aligned} \Pi_{VV} - \Pi_{AA} &= \frac{1}{3} \sum_\epsilon \int \frac{d^4 p}{i(2\pi)^4} \frac{N_c}{2} \text{tr} \left[\not{\epsilon} \chi^{(J)}(p; q, \epsilon) - \not{\epsilon} \gamma_5 \chi^{(A)}(p; q, \epsilon) \right], \\ &= \frac{N_c}{\pi^3} \int_0^\infty du \int_0^\infty dx x^2 \left[- \left(\chi_1^{(V)}(u, x; Q) + \chi_1^{(A)}(u, x; Q) \right) \right. \\ &\quad \left. + \frac{x^2}{3} \left(\chi_6^{(V)}(u, x; Q) + \chi_6^{(A)}(u, x; Q) \right) \right]. \end{aligned} \quad (4.13)$$

We note that, although either Π_{VV} or Π_{AA} is logarithmically divergent quantity, the difference $\Pi_{VV} - \Pi_{AA}$ becomes finite due to the cancellation of the divergence ensured by the chiral symmetry.

5 Inhomogeneous Bethe-Salpeter equation

In this section we introduce the inhomogeneous Bethe-Salpeter (IBS) equation from which we calculate the BS amplitude defined in the previous section.

The IBS equation is the self-consistent equation for the BS amplitude $\chi^{(J)}$, and it is expressed as (see Fig. 2 for graphical expression)

$$T(p; q) \chi^{(J)}(p; q, \epsilon) = \epsilon \cdot G^{(J)} + K(p; k) * \chi^{(J)}(k; q, \epsilon). \quad (5.1)$$

The kinetic part T is given by

$$T(p; q) = S_F^{-1}(p + q/2) \otimes S_F^{-1}(p - q/2), \quad (5.2)$$

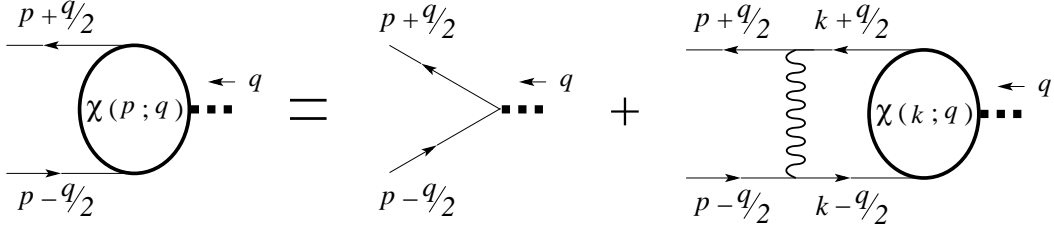


Figure 2: A graphical expression of the IBS equation in the (improved) ladder approximation.

where S_F is the full fermion propagator $iS_F^{-1}(p) = \not{p} - \Sigma(p)$. (Note that wave function renormalization factor $A(p)$ becomes unity when we adopt the Landau gauge.) The BS kernel K in the improved ladder approximation is expressed as

$$K(p; k) = \frac{N_c^2 - 1}{2N_c} \frac{\bar{g}^2(p, k)}{-(p - k)^2} \left(g_{\mu\nu} - \frac{(p - k)_\mu (p - k)_\nu}{(p - k)^2} \right) \cdot \gamma^\mu \otimes \gamma^\nu, \quad (5.3)$$

where $\bar{g}(p, k)$ is the running coupling of QCD whose explicit form will be shown later. In the above expressions we used the tensor product notation

$$(A \otimes B) \chi = A \chi B, \quad (5.4)$$

and the inner product notation

$$K(p; k) * \chi^{(J)}(k; q, \epsilon) = \int \frac{d^4 k}{i(2\pi)^4} K(p, k) \chi(k; q). \quad (5.5)$$

The mass function of the quark propagator is obtained from the SD equation (see appendix A) :

$$\Sigma(p) = K(p, k) * iS_F(p). \quad (5.6)$$

It should be stressed that we must use the same kernel $K(p, k)$ as that used in the IBS equation for consistency with the chiral symmetry [42, 43]. Numerical method for solving the SD equation and the IBS equation are shown in appendix B and appendix C, respectively.

6 Numerical results

In this section, we show the results of the calculations for f_π , \hat{S} , and Δm_π^2 in the large N_f QCD near the chiral phase transition point. The procedure of the calculation is as follows. First, we solve the IBS equation and the SD equation simultaneously, and obtain BS amplitude $\chi^{V,A}$. (Details of numerical methods to solve the SD and the IBS equations are shown in appendix B and appendix C.) Then, by closing the fermion legs of BS amplitudes, we obtain current correlators $\Pi_{VV}(Q^2)$ and $\Pi_{AA}(Q^2)$. (See section 4.) Once we obtain $\Pi_{VV}(Q^2)$ and $\Pi_{AA}(Q^2)$, we calculate f_π^2 , \hat{S} , and Δm_π^2 from the relations in Eqs. (3.3), (3.5) and (3.6).

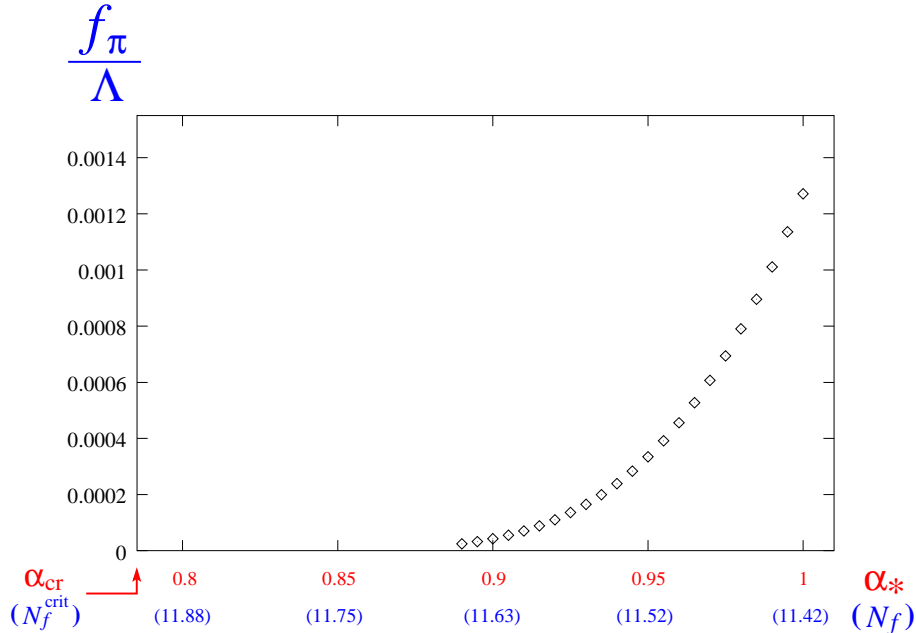


Figure 3: Values of f_π calculated from Eq. (3.3) for several values of α_* in the range of $\alpha_* \in [0.89 : 1]$ (indicated by \diamond). Values of N_f corresponding to each α_* are shown in parenthesis.

6.1 Critical behavior of f_π in the large N_f QCD

In Fig. 3, we plot f_π for several values of α_* in the range of $\alpha_* \in [0.89 : 1]$. Note that we use α_* instead of N_f as an input parameter, because once we choose a value of N_f , the value of α_* is uniquely determined from Eq. (2.3). $\alpha_* = \alpha_{\text{cr}}$ implies $N_f = 11.91$. In Fig. 3, we have shown corresponding values of N_f in the parenthesis. From this figure, we can see that f_π goes to zero when we reduce the value of α_* to its critical value $\alpha_{\text{cr}} \simeq \pi/4$ (or increase the value of N_f to its critical value $N_f^{\text{crit}} \simeq 4N_c$), which is consistent with the chiral phase transition described in section 2. Furthermore, the scaling behavior is identified as essential singularity type,

$$f_\pi = p \Lambda \exp\left(-\frac{q}{\sqrt{\frac{\alpha_*}{\alpha_{\text{cr}}} - 1}}\right) \quad (6.1)$$

with $p = 15.1$ and $q = 4.9$ as the best fit. This is similar to the case with constant coupling with sharp cutoff at Λ [21]:⁵

$$f_\pi = d \Lambda \exp\left(-\frac{\pi}{\sqrt{\frac{\alpha_*}{\alpha_{\text{cr}}} - 1}}\right), \quad (d \simeq 1.5). \quad (6.2)$$

⁵At first glance there is some numerical difference between the case with a constant coupling and that with a two-loop coupling, which is mainly due to the different meanings of Λ for these two cases. Actually, such a superficial difference also takes place for $m = \Sigma(m^2)$ which is essentially proportional to f_π , with the ratios being the same in both cases.

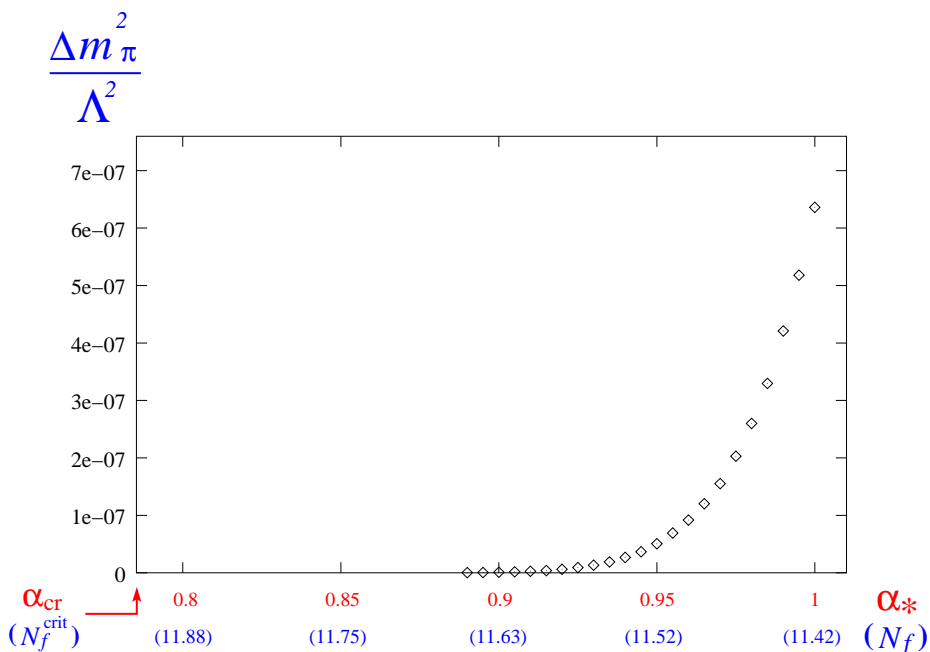


Figure 4: Values of Δm_π^2 calculated from Eq. (3.6) for several values of α_* in the range of $\alpha_* \in [0.89 : 1]$ (indicated by \diamond).

6.2 Critical behavior of Δm_π^2 in the large N_f QCD

In Fig. 4, we plot Δm_π^2 calculated for several values of α_* in the range of $\alpha_* \in [0.89 : 1]$. In our numerical calculation of Δm_π^2 , we introduced the numerical cutoff Λ_{Num}^2 :

$$\frac{\Pi_{V-A}(Q^2 = \Lambda_{\text{Num}}^2)}{\Pi_{V-A}(Q^2 = 0)} = \frac{1}{50} \quad (6.3)$$

for the integration of $\Pi_{V-A}(Q^2) \equiv [\Pi_{VV} - \Pi_{AA}](Q^2)$ in Eq. (3.6) as follows:

$$\Delta m_\pi^2 = \frac{3\alpha_{em}}{4\pi f_\pi^2} \int_0^{\Lambda_{\text{num}}^2} dQ^2 \Pi_{V-A}(Q^2). \quad (6.4)$$

We shall discuss later inclusion of the contributions from $\Lambda_{\text{Num}}^2 < Q^2 < \Lambda^2$.

From this figure, we see that Δm_π^2 vanishes to zero when approaching the chiral phase transition point from the broken phase. To see the scaling behavior of Δm_π^2 near the phase transition point, we plot the values of $\Delta m_\pi^2 / f_\pi^2$ in Fig. 5 for several values of α_* in the range of $\alpha_* \in [0.89 : 1]$. From this figure, we can see that $\Delta m_\pi^2 / f_\pi^2$ in the large N_f QCD near the phase transition point gradually increases

$$\frac{\Delta m_\pi^2}{f_\pi^2} = 0.4 \quad \text{to} \quad 0.6, \quad (6.5)$$

in the range of $\alpha_* \in [0.89 : 1]$ investigated here.

The most outstanding feature of the value in Eq. (6.5) is that it is rather large compared with that of the real-life QCD [23],

$$\left. \frac{\Delta m_\pi^2}{f_\pi^2} \right|_{\text{real-life QCD}} \simeq 0.123, \quad (6.6)$$

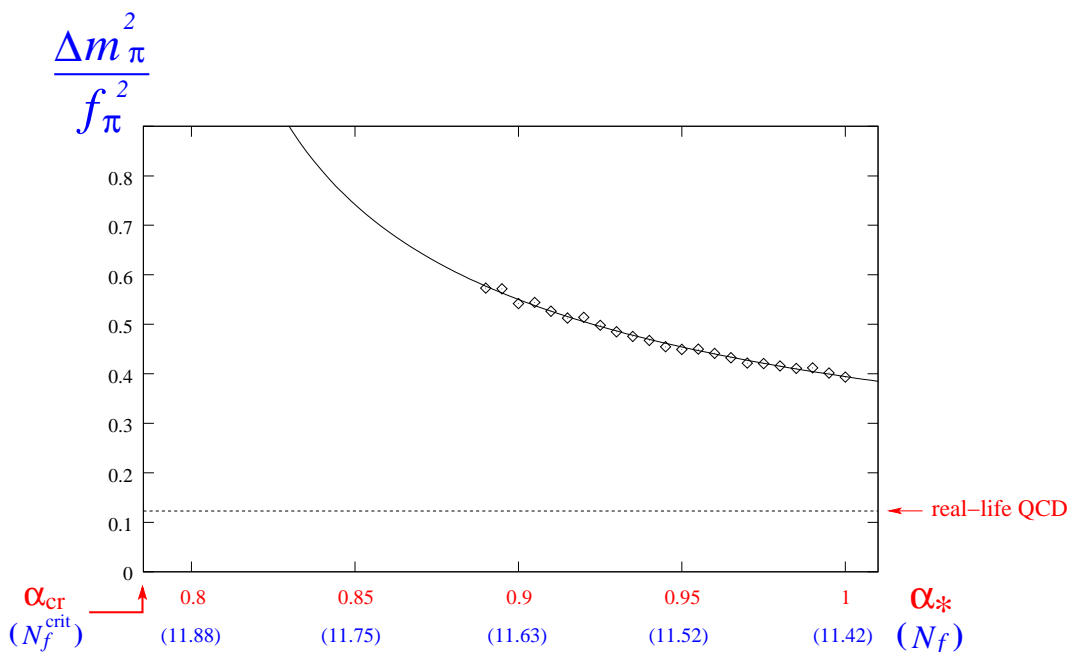


Figure 5: Values of $\Delta m_\pi^2/f_\pi^2$ for several values of α_* in the range of $\alpha_* \in [0.89 : 1]$ (indicated by \diamond). Solid line shows the fitting function $I(\alpha_*)$ given in Eq.(6.11). Value of $\Delta m_\pi^2/f_\pi^2$ of the real-life QCD calculated in Ref. [23] is also shown in the figure. Here, we used the data with the infrared cutoff parameter of the running coupling $t_F = 0.04$.

calculated in the same method with the numerical cutoff Λ_{Num} defined as Eq. (6.3) (The experimental value: $\Delta m_\pi^2/f_\pi^2 = 0.148 \pm 0.001$). We shall argue that this enhancement reflects the large anomalous dimension $\gamma_m \simeq 1$ characteristic to the walking/conformal (scale-invariant) technicolor [13].

6.3 Inverse square root scaling of Δm_π^2

To see the cause of this enhancement of $\Delta m_\pi^2/f_\pi^2$ let us compare the behavior of $\Pi_{V-A}(Q^2)/f_\pi^2$ versus Q^2/f_π^2 of the large N_f QCD with that of the real-life QCD, see Fig. 6. It is clear from Fig. 6 that $\Pi_{V-A}(Q^2)/f_\pi^2$ in the large N_f QCD is more slowly damping in high Q^2 than that in the real-life QCD, which consequently yields bigger area integral in Fig. 6 than that of the real-life QCD. This is the cause of the enhancement of $\Delta m_\pi^2/f_\pi^2$.

To understand the slow damping it is convenient to divide the integral region of the DGMLY sum rule (“third Weinberg sum rule”), Eq. (3.6), into high and low energy regions as

$$\begin{aligned} \Delta m_\pi^2 &= \frac{3\alpha_{em}}{4\pi f_\pi^2} \left(\int_0^{\Lambda_\chi^2} dQ^2 + \int_{\Lambda_\chi^2}^\infty dQ^2 \right) \Pi_{V-A}(Q^2) \\ &\equiv \Delta m_{\pi(\text{IR})}^2 + \Delta m_{\pi(\text{UV})}^2, \end{aligned} \quad (6.7)$$

where Λ_χ was introduced in such a way that, in the high energy region $Q^2 > \Lambda_\chi^2$, the behavior of $[\Pi_{VV}(Q^2) - \Pi_{AA}(Q^2)]$ is well approximated by the one obtained from

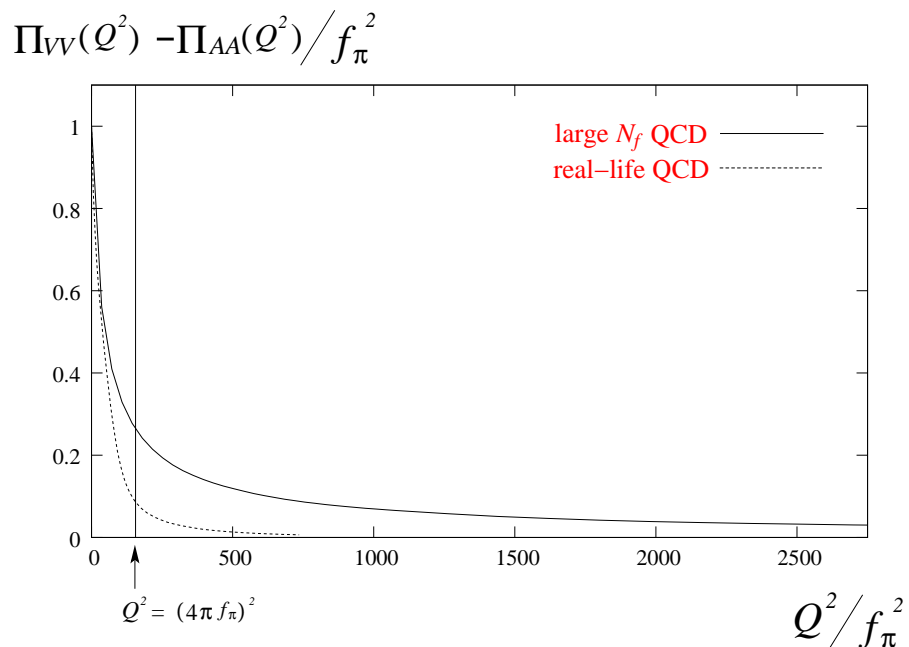


Figure 6: Comparison of $\Pi_{V=A}(Q^2)$ between the large N_f QCD and the real-life QCD. Solid line indicates $\Pi_{V=A}(Q^2)$ in the large N_f QCD for $\alpha_* = 0.90$, while dotted line indicates $\Pi_{V=A}(Q^2)$ in the real-life QCD ($N_f = 3$). In this figure, both horizontal and vertical axes are normalized by the respective value of f_π^2 . $\Pi_{V=A}(Q^2)$ in the real-life QCD was calculated in Ref. [23]. Here, we used the data with the infrared cutoff parameter of the running coupling $t_F = 0.04$, which reproduce the QCD S parameter and Δm_π^2 in good agreement with experiments [23].

the operator product expansion (OPE) technique in the high energy region (see, e.g., Ref. [44]). In the real-life QCD such a scale is given by $\Lambda_\chi = 4\pi f_\pi \sim 1.1\text{GeV} (> \Lambda_{\text{QCD}})$, above which ($Q^2 > \Lambda_\chi^2$) the QCD gauge coupling α becomes small enough for the OPE to be obviously valid. On the other hand, in the large N_f QCD the QCD gauge coupling α is almost constant (walking) over the range $\Lambda_\chi^2 < Q^2 < \Lambda^2$ and is not very small (of order 1), where $\Lambda_\chi = 4\pi f_\pi \simeq 4.7m (\ll \Lambda)$ in the large N_f QCD [21] (m is the dynamical mass of the fermion). Nevertheless we expect that the OPE is still operative as was discussed [45] in the walking/conformal (scale-invariant) technicolor. Note that OPE obviously breaks down for $Q^2 < m^2$ since the gauge coupling blows up due to the fact that the fermion which acquired mass m gets decoupled from the beta function, while for $Q^2 > \Lambda^2$ OPE is trivially valid (with vanishing anomalous dimension) since the gauge coupling is negligibly small due to the strong asymptotic freedom (see Fig. 1).

Then the OPE dictates that the correlator $\Pi_{VV}(Q^2) - \Pi_{AA}(Q^2)$ behaves as for large Q^2 :

$$\Pi_{V-A}(Q^2) \equiv \Pi_{VV}(Q^2) - \Pi_{AA}(Q^2) \sim \frac{\langle \bar{q}q \rangle_{\Lambda_\chi}^2}{Q^{4-2\gamma_m}} \text{ for } Q^2 > \Lambda_\chi^2 \sim (4\pi f_\pi)^2, \quad (6.8)$$

where γ_m is the anomalous dimension, and $\langle \bar{q}q \rangle_{\Lambda_\chi}$ is $\bar{q}q$ condensation at the scale of Λ_χ .⁶ Note that the large N_f QCD is a walking theory characterized by $\gamma_m \simeq 1$ [13] which was confirmed by explicit calculation [21]. On the other hand, in the real-life QCD we have $\gamma_m \simeq 0$ up to logarithm.⁷ Eq. (6.8) roughly reflects the slowly damping behavior of $(\Pi_{VV}(Q^2) - \Pi_{AA}(Q^2))/f_\pi^2$ of the large N_f QCD compared with the real-life QCD in Fig. 6 at least in the high energy region $Q^2 > \Lambda_\chi^2$. In fact, $1/Q^2$ damping for $\gamma_m \simeq 1$ yields the integral for $\Delta m_{\pi(\text{UV})}^2$ in Eq. (6.7) a logarithmic divergence which is cutoff by Λ^2 beyond which the integrand changes into the $1/Q^4$ damping due to the strongly asymptotic freedom there. Then the enhancement by the large anomalous dimension $\gamma_m \simeq 1$ reads roughly

$$\frac{\Delta m_{\pi(\text{UV})}^2}{f_\pi^2} \sim \ln(\Lambda^2/\Lambda_\chi^2) \sim \frac{2q}{\sqrt{\frac{\alpha_*}{\alpha_{\text{cr}}} - 1}} - 2 \ln(4\pi p), \quad (6.9)$$

where we have used Eq. (6.1), with $p \simeq 15.1$, $q \simeq 4.9$. This implies that $\Delta m_{\pi(\text{UV})}^2/f_\pi^2$ *diverges as inverse square root scaling*, when we approach to the critical point. As to the infrared contributions to $\Delta m_{\pi(\text{UV})}^2/f_\pi^2$, we can see from the areas divided by the vertical line of $Q^2 = (4\pi f_\pi)^2$ in Fig. 6 that, even evaluated with $\Lambda_{\text{Num}} (\ll \Lambda)$, $\Delta m_{\pi(\text{UV})}^2/f_\pi^2$ dominates $\Delta m_{\pi(\text{IR})}^2/f_\pi^2$, 70% to 30%, already at $\alpha_* = 0.90$, in sharp contrast to the real-life QCD where UV contributions vs IR contributions are opposite ratio: 20% to 80%. We expect that as we approach to the critical point $\alpha_* \rightarrow \alpha_{\text{cr}}$, the cutoff Λ^2 of the integral region in Fig. 6 grows rapidly even if the damping slope

⁶Making explicit the dimensions, Eq. (6.8) reads $\Pi_{V-A}(Q^2) \sim (\Lambda_\chi)^2 \cdot (\Lambda_\chi/Q)^{4-2\gamma_m}$.

⁷In the real-life QCD the OPE in Eq. (6.8) actually has a logarithmic factor $\alpha(Q^2) \times (\ln(Q^2/\Lambda_{\text{QCD}}^2))^A$, with $A = 24/(33-2N_f) = 8/9$ ($N_f = 3$), which however reads $(\ln(Q^2/\Lambda_{\text{QCD}}^2))^{-1/9}$ and yields only a negligible Q^2 dependence.

were unchanged, since the figure is drawn in the unit of f_π^2 which actually vanishes exponentially with respect to Λ^2 . Then $\Delta m_{\pi(\text{UV})}^2/f_\pi^2 \rightarrow \Delta m_\pi^2/f_\pi^2$ near the critical point. Hence we conclude an inverse square root scaling for $\Delta m_\pi^2/f_\pi^2$:

$$\frac{\Delta m_\pi^2}{f_\pi^2} \sim \frac{1}{\sqrt{\frac{\alpha_*}{\alpha_{\text{cr}}} - 1}}. \quad (6.10)$$

This is compared with our numerical data in Fig. 5, where the solid line is a fitting function as

$$I(\alpha_*) = m \times \left(\frac{2\pi}{\sqrt{\frac{\alpha_*}{\alpha_{\text{cr}}} - 1}} + n \right) \quad (6.11)$$

which was obtained by fitting it to the calculated data. Best fitted values for m and n are found to be $m \simeq 0.035$ and $n \simeq -0.82$. Here we note that Fig. 5 was given by the contributions from the region $0 < Q^2 < \Lambda_{\text{Num}}^2$ instead of $0 < Q^2 < \Lambda^2$. We shall later discuss additional contributions from $\Lambda_{\text{Num}}^2 < Q^2 < \Lambda^2$ which may be estimated analytically based on the walking behavior of $\Pi_{V-A}(Q^2) \sim 1/Q^2$. In spite of lacking the contributions from $\Lambda_{\text{Num}}^2 < Q^2 < \Lambda^2$, our data nevertheless show an enhanced mass of pseudo NG bosons reflecting an inverse square root scaling of the walking theory:

$$\frac{\Delta m_\pi^2}{f_\pi^2} \simeq I(\alpha_*) \sim \frac{0.07\pi}{\sqrt{\frac{\alpha_*}{\alpha_{\text{cr}}} - 1}} \quad (6.12)$$

near the critical point $\alpha_* = \alpha_*(N_f, N_c) \rightarrow \alpha_{\text{cr}}$.

In passing, Eq. (6.8) further suggests that

$$Q^4 \Pi_{V-A}(Q^2) \Big|_{\text{real-lifeQCD}} \sim Q^2 \Pi_{V-A}(Q^2) \Big|_{\text{large } N_f \text{ QCD}} \sim \text{const. for } Q^2 > \Lambda_\chi^2. \quad (6.13)$$

It is amusing to note that the first relation seems to hold numerically all the way down to the infrared region $Q^2 < \Lambda_\chi^2$ where the OPE as it stands obviously breaks down, see Fig. 7.⁸ The remnant of the OPE carrying the information of the anomalous dimension seems to persist as the difference of power behaviors according to the difference of the anomalous dimension even in the IR region.

6.4 Calculation of S parameter

In Fig. 8, we plot \hat{S} for several values of α_* in the range of $\alpha_* \in [0.89 : 1]$. There is an ambiguity how many data points we use when we calculate the differential coefficient of $\Pi_{VV}(Q^2) - \Pi_{AA}(Q^2)$ at $Q^2 = 0$. We calculate it by using 3, 4, 5, and 7 data points, and resultant values of \hat{S} are indicated in Fig. 8 by \circ , \times , $*$, and \bullet , respectively. The value of \hat{S} is sensitive to the choice of number of data points we use, however, it

⁸The line of the large N_f QCD in Fig. 7 does not yet level off to a constant value up till this momentum region. This is consistent with Ref. [21] where the numerical values of γ_m calculated for the values of α_* still away from the critical coupling are slightly larger than 1.

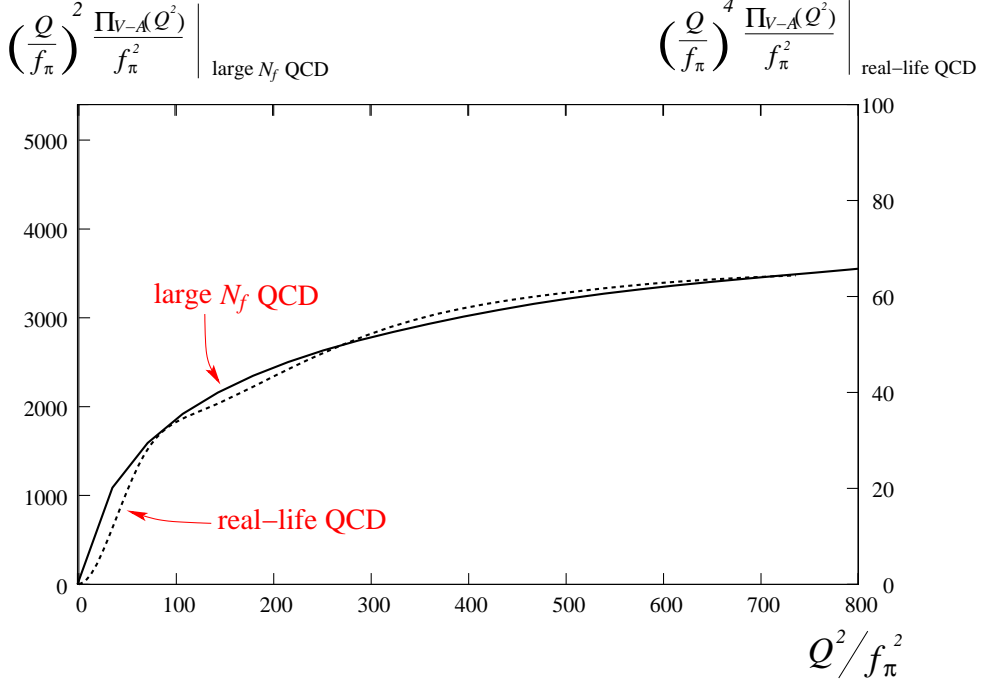


Figure 7: Comparison between $\left(\frac{Q}{f_\pi}\right)^2 \cdot \Pi_{V-A}(Q^2)/f_\pi^2$ in the large N_f QCD with $\alpha_* = 0.90$ (solid line) and $\left(\frac{Q}{f_\pi}\right)^4 \cdot \Pi_{V-A}(Q^2)/f_\pi^2$ in real-life QCD with $t_F = 0.04$ calculated in Ref. [23] (dashed line).

converges as we increase the number of data points. From this figure, we see that \hat{S} in the large N_f QCD near the phase transition point takes values

$$\hat{S} = 0.25 \quad \text{to} \quad 0.30, \quad (6.14)$$

which are slightly smaller (but without much difference) than that of the real-life QCD calculated in the same method, $\hat{S} \simeq 0.33$, and have a tendency decreasing as we approach the critical point.

Although our results are still larger than the estimation from the perturbative calculation [26], $\hat{S}_{\text{pert}} = \frac{N_c}{6\pi} \simeq 0.16$, at least in the range of $\alpha_* \in [0.89 : 1]$ investigated here, a simple-minded extrapolation seems to suggest that it might get to smaller values in the range of $\alpha_* \in [\alpha_{\text{cr}} : 0.89]$. Although in the present analysis we were not able to solve the IBS equation in the range of $\alpha_* \in [\alpha_{\text{cr}} : 0.89]$ because the numerical calculation near the critical point is quite difficult, it will motivate future work to extend the analysis to the region closer to the critical point and see whether or not \hat{S} gets dramatic reduction near the critical point.

In passing, here we note an interesting correlation between \hat{S} and the numerical value of Δm_π^2 with an artificial cutoff Λ_{Num} . In Fig. 6 $\Delta m_\pi^2/f_\pi^2$ is proportional to the area surrounded by the vertical axis, horizontal axis, the curve of $(\Pi_{VV}(Q^2) - \Pi_{AA}(Q^2))/f_\pi^2$ and the line of the cutoff $Q^2 = \Lambda_{\text{Num}}^2$ which does depend on the slope of the current correlators $\Pi_{V-A}(Q^2)$ at $Q^2 = 0$, namely the \hat{S} . When \hat{S} gets smaller, Λ_{Num}^2 defined by Eq. (6.3) necessarily increases and so does $\Delta m_\pi^2/f_\pi^2$ in our numerical

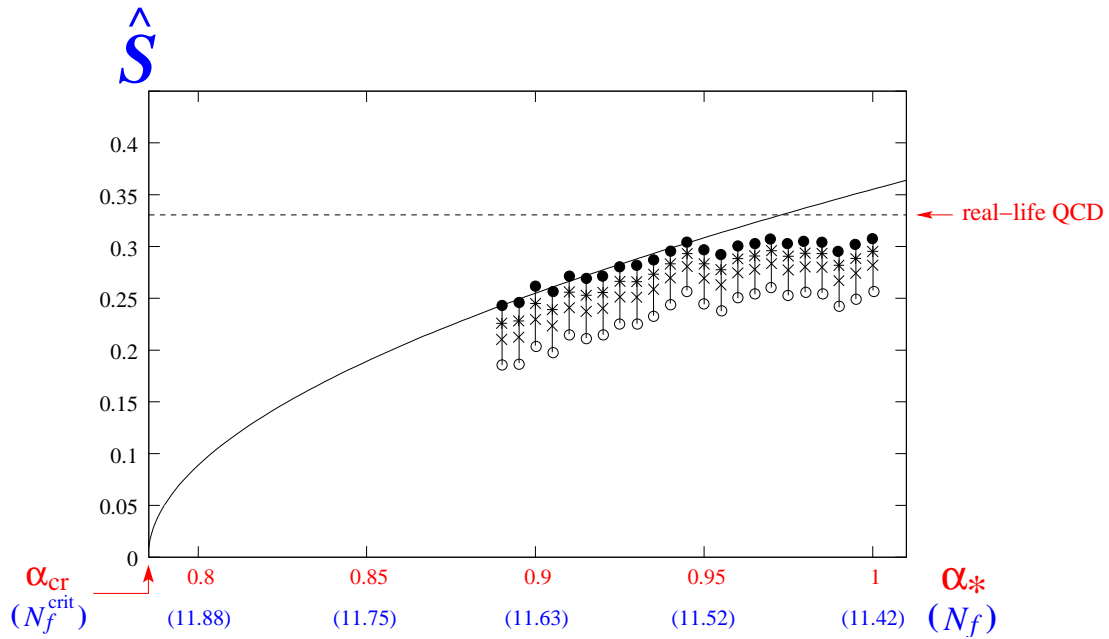


Figure 8: Values of \hat{S} calculated from Eq. (3.5) for several values of α_* in the range of $\alpha_* \in [0.89 : 1]$. Points indicated by \circ , \times , $*$, and \bullet are values of \hat{S} calculated by using 3, 4, 5, and 7 data points of $\Pi_{VV} - \Pi_{AA}$, respectively. Solid line shows the form of function $J(\alpha_*)$ in Eq. (6.16). Value of \hat{S} of the real-life QCD calculated in Ref. [23] is also shown in the figure. Here, we used the data with the infrared cutoff parameter of the running coupling $t_F = 0.04$.

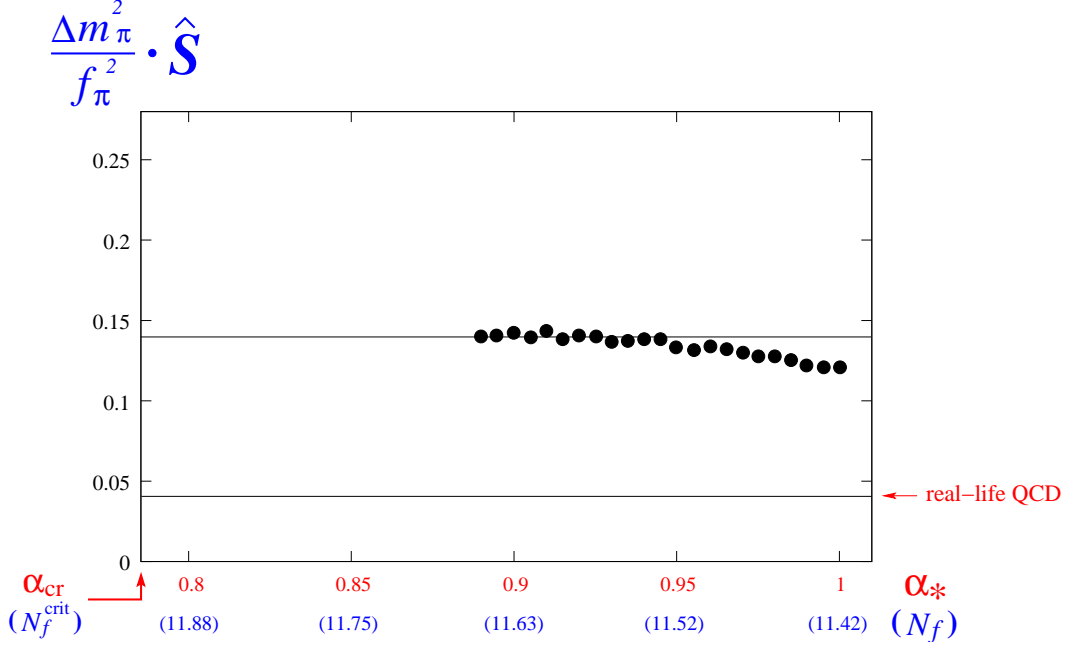


Figure 9: Values of $\hat{S} \cdot \Delta m_\pi^2 / f_\pi^2$ for several values of α_* . Solid line shows the value obtained by averaging the values of data below $\alpha_* = 0.95$ as shown in Eq. (6.15). Value of $\hat{S} \cdot \Delta m_\pi^2 / f_\pi^2$ of the real-life QCD calculated in Ref. [23] is also shown in the figure. Here, we used the data with the infrared cutoff parameter of the running coupling $t_F = 0.04$.

calculations.⁹ In Fig. 9 we plotted $S \cdot \Delta m_\pi^2 / f_\pi^2$ for several values of α_* in the range of $\alpha_* \in [0.89 : 1]$. This product is almost constant near the critical point and seems to stay as a constant also in the region $\alpha_* \in [\alpha_{\text{cr}} : 0.89]$:

$$\frac{\Delta m_\pi^2}{f_\pi^2} \times \hat{S} \sim \text{constant} \simeq 0.14 \quad (\alpha_* \leq 0.95) \quad (6.15)$$

From this we might infer the behavior of \hat{S} as an inverse function of $\Delta m_\pi^2 / f_\pi^2$ given in Eq. (6.11):

$$\hat{S} \simeq J(\alpha_*) = \frac{0.14}{I(\alpha_*)} = 4 \left(\frac{2\pi}{\sqrt{\frac{\alpha_*}{\alpha_{\text{cr}}} - 1}} - 0.82 \right)^{-1}. \quad (6.16)$$

However, this argument is totally based on the assumption that $\Lambda_{\text{Num}}^2 / \Lambda_\chi^2$ scales in the same way as $\Lambda^2 / \Lambda_\chi^2$ does in a Miransky scaling. Although there is no solid theoretical support for such a continuation of the Miransky scaling in the more vicinity of the critical point as we discuss later, $\Lambda_{\text{Num}}^2 / \Lambda_\chi^2$ imitates the Miransky scaling as far as the region we explicitly calculated is concerned. Thus, it is certainly interesting to check in future the above square root scaling of \hat{S} by directly computing \hat{S} in the region closer to the critical point.

⁹This is contrasted to the case where our integration is cut off at Λ^2 (instead of Λ_{Num}^2) which has no correlation with the slope at $Q^2 = 0$.

In Ref. [28], it was argued that there arises a negative contribution proportional to the dynamical mass of the fermion due to the walking behavior of the running coupling, and that the S parameter in the large N_f QCD could be much reduced relative to that in QCD-like theories. However, as far as we analyzed in the present paper S does not seem to take a negative value.

7 Conclusion and Discussions

In this paper, in the framework of the SD and the IBS equations, we calculated f_π , \hat{S} , and Δm_π^2 on the same footing in the large N_f QCD, through the difference between the vector current correlator Π_{VV} and the axial-vector current correlator Π_{AA} .

When the chiral phase transition point is approached from the broken phase, $\alpha_* \rightarrow \alpha_{\text{cr}}$, f_π and Δm_π^2 go to zero both with the essential-singularity scaling (Miransky scaling), whereas the ratio $\Delta m_\pi^2/f_\pi^2$ increases and actually scales as an inverse square root (Fig. 5 and Eq. (6.12)):

$$\frac{\Delta m_\pi^2}{f_\pi^2} \sim \frac{0.07\pi}{\sqrt{\frac{\alpha_*}{\alpha_{\text{cr}}} - 1}}. \quad (7.1)$$

Thus the radiative mass of the pseudo NG boson can be dramatically enhanced compared with the conventional estimate of the techni pseudo's based on a simple scale-up of QCD with a factor scaling of N_f and N_c .

Here we should mention that our numerical estimate of $\Delta m_\pi^2/f_\pi^2$ was done on the integral for the region $0 < Q^2 < \Lambda_{\text{Num}}^2$ instead of $0 < Q^2 < \Lambda^2$, since it is rather difficult to estimate them by directly solving the IBS equation numerically including larger Q^2 regions. We now discuss the additional contributions from $\Lambda_{\text{Num}}^2 < Q^2 < \Lambda^2$ through an analytical estimate, instead of directly solving the IBS equation, based on the observed walking behavior of the current correlators $\Pi_{V-A}(Q^2) \sim 1/Q^2$. We divide the integral for Δm_π^2 as

$$\Delta m_\pi^2 = \frac{3\alpha_{em}}{4\pi f_\pi^2} \left(\int_0^{\Lambda_{\text{Num}}^2} dQ^2 + \int_{\Lambda_{\text{Num}}^2}^{\Lambda^2} dQ^2 \right) [\Pi_{V-A}(Q^2)], \quad (7.2)$$

$$\equiv \Delta m_{\pi(\text{Num})}^2 + \Delta m_{\pi(\text{UV}>)}^2. \quad (7.3)$$

By definition of Λ_{Num} in Eq. (6.3) we have

$$\frac{\Pi_{V-A}(Q^2)}{f_\pi^2} = \frac{1}{50} \frac{\Lambda_{\text{Num}}^2}{Q^2} \quad (\Lambda_{\text{Num}}^2 < Q^2 < \Lambda^2), \quad (7.4)$$

which is substituted into the above $\Delta m_{\pi(\text{UV}>)}^2$:

$$\frac{\Delta m_{\pi(\text{UV}>)}^2}{f_\pi^2} = \frac{1}{50} \frac{3\alpha_{em}}{4\pi} \frac{\Lambda_{\text{Num}}^2}{f_\pi^2} \ln \left(\frac{\Lambda^2}{\Lambda_{\text{Num}}^2} \right). \quad (7.5)$$

Values of $(\Lambda_{\text{Num}}^2/\Lambda_\chi^2)$ and $(\Lambda^2/\Lambda_{\text{Num}}^2)$ are summarized in Table 1. Considering the definition of Λ_χ ($\equiv 4\pi f_\pi$) and the fact that the scaling of f_π/Λ is identified

α_*	$\Lambda_{\text{Num}}^2/\Lambda_\chi^2$	$\Lambda^2/\Lambda_{\text{Num}}^2$	α_*	$\Lambda_{\text{Num}}^2/\Lambda_\chi^2$	$\Lambda^2/\Lambda_{\text{Num}}^2$
0.890	28	3.8×10^5	0.950	21	2.7×10^3
0.895	29	2.0×10^5	0.955	21	1.9×10^3
0.900	26	1.3×10^5	0.960	21	1.4×10^3
0.905	27	7.6×10^4	0.965	21	1.1×10^3
0.910	26	4.8×10^4	0.970	20	8.8×10^2
0.915	25	3.3×10^4	0.975	20	6.7×10^2
0.920	26	2.0×10^4	0.980	20	5.2×10^2
0.925	25	1.4×10^4	0.985	19	4.1×10^2
0.930	23	1.0×10^4	0.990	19	3.3×10^2
0.935	23	7.0×10^3	0.995	18	2.7×10^2
0.940	23	4.9×10^3	1.000	18	2.2×10^2
0.945	22	3.6×10^3			

Table 1: Values of $(\Lambda_{\text{Num}}^2/\Lambda_\chi^2)$ and $(\Lambda^2/\Lambda_{\text{Num}}^2)$ for several values of α_* .

as Miransky scaling (see Eq. (6.9) and Fig. 3), we can understand that Λ^2/Λ_χ^2 also shows the (inverse) Miransky scaling. Λ^2/Λ_χ^2 is viewed as a product of $\Lambda^2/\Lambda_{\text{Num}}^2$ and $\Lambda_{\text{Num}}^2/\Lambda_\chi^2$, the former becoming more prominent as we get closer to the critical point. This implies that cutting off the integral for Δm_π^2 at Λ_{Num}^2 does not reproduce main part of the walking theory and hence does not yield a good approximation, in sharp contrast to the case of the real-life QCD. Nevertheless $\Lambda_{\text{Num}}^2/\Lambda_\chi^2$ is also growing as we get closer to the critical point, which corresponds to decreasing of \hat{S} . This actually imitates the Miransky scaling in such a way that $\Delta m_{\pi(\text{Num})}^2$ behaves as if in an inverse square root scaling observed in Fig. 5 and Eq. (6.12).

In Fig. 10, we plot the values of $\Delta m_{\pi(\text{Num})}^2$, $\Delta m_{\pi(\text{UV})}^2$, and Δm_π^2 in the unit of f_π^2 for several values of α_* . As was noted above, the additional contributions from $\Lambda_{\text{Num}}^2 < Q^2 < \Lambda^2$ is much larger than those from $Q^2 < \Lambda_{\text{Num}}^2$ which we calculated numerically, since $\Lambda^2/\Lambda_{\text{Num}}^2 \gg \Lambda_{\text{Num}}^2/\Lambda_\chi^2$ (see Table 1) in the walking regions. The fitting function for total Δm_π^2 reads $m \simeq 0.042$ and $n \simeq -0.268$ in the parameterization of Eq. (6.11). This figure clearly shows that the contribution from $Q^2 > \Lambda_{\text{Num}}^2$ dominates the scaling of total Δm_π^2 . When it is applied for a popular technicolor model (one-family model) of Farhi-Susskind [12], with $\Lambda_\chi = 4\pi f_\pi \sim 4\pi \times 123\text{GeV}$, we are interested in the region $\Lambda < \Lambda_{\text{ETC}} \sim 10^3\text{TeV}$ and hence $\Lambda/\Lambda_\chi \sim 6.5 \times 10^2$ (we are using $N_{\text{TC}} = 3$ in this case). This roughly corresponds to $\alpha_* = 0.975$ in Table 1 and $\Delta m_\pi^2/f_\pi^2 = 1.12$, about 9 times larger than the value estimated in the real-life QCD $\Delta m_\pi^2/f_\pi^2 \simeq 0.123$ [23] (experimental value $\Delta m_\pi^2 = 0.148 \pm 0.001$) in the same method. This suggests that the radiative mass of the pseudo NG bosons in the walking technicolor could be enhanced by a factor 3 compared with a simple scale up of the QCD. The typical estimate of 100GeV mass range [12] would be boosted to 300GeV range, which could be of phenomenological relevance.

As to \hat{S} , our numerical result showed $\hat{S} \simeq 0.25 - 0.30$ which is somewhat smaller than that in the real-life QCD and indicated a decreasing tendency as we approach the critical point. Here we note that there is a subtlety to evaluate the slope of $\Pi_{V-A}(Q^2)$

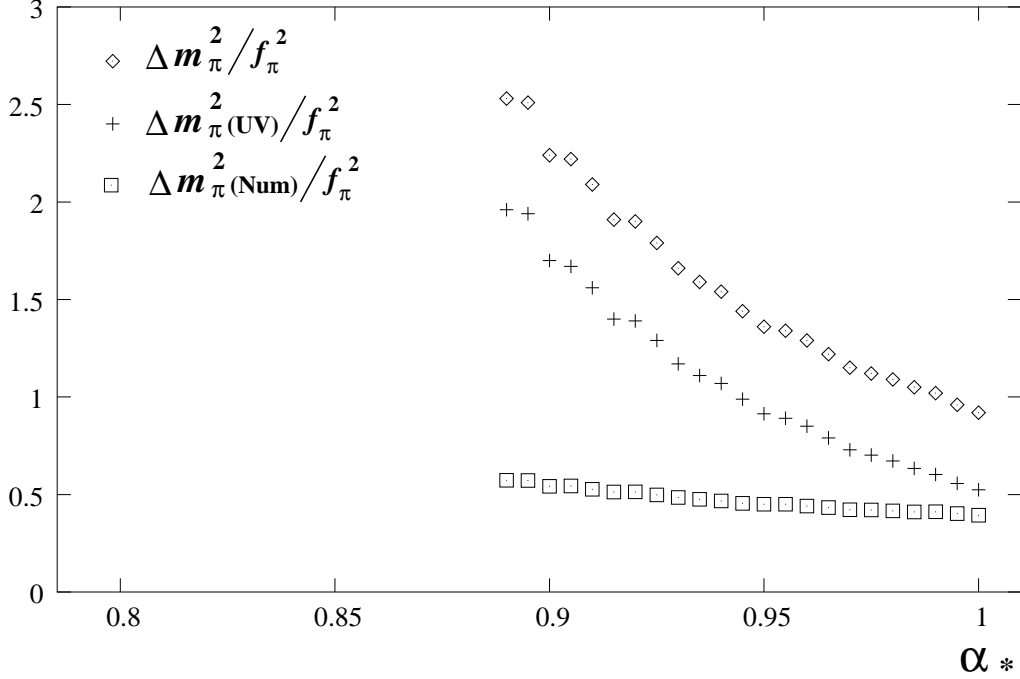


Figure 10: Values of $\Delta m_\pi^2(\text{Num})$, $\Delta m_\pi^2(\text{UV})$, and Δm_π^2 in the unit of f_π^2 for several values of α_* .

at $Q^2 = 0$ numerically. To check this subtlety we compute another quantity \hat{S}_* :

$$\hat{S}_* \equiv -4\pi \frac{\Pi_{V-A}(Q^2 = f_\pi^2) - \Pi_{V-A}(Q^2 = 0)}{f_\pi^2}, \quad (7.6)$$

which is similar to the popular definition of S except for the point that ours is defined for the space-like momentum instead of the time-like one. Numerical results for several values of α_* are summarized in Table 2.

In Fig. 11, we plotted the values of \hat{S}_* shown in Table 2. The data in the previous definition are also plotted in this figure. The result is somewhat larger than the value in the previous method and seems to indicate slower decreasing behavior than the previous one as we approach the critical point. Thus, up to this subtlety, it seems unlikely that \hat{S} is dramatically reduced in the large N_f QCD at least in the region we calculated. At any rate it is highly desirable to extend our analysis to closer region to the critical point and check by explicit computation whether or not our conclusion in this paper persists there.

In the present analysis, we only considered $SU(N_c)$ gauge theory with $N_c = 3$ (with N_f flavors). This is because, by taking $N_c = 3$, it became possible to compare the result of the large N_f $SU(N_c)$ gauge theory with usual QCD ($N_c = 3, N_f = 3$), and see the difference of dynamics which is caused by the difference of the number of flavors. However, there is no reason to prohibit us from considering the large N_f $SU(N_c)$ gauge theory with $N_c \neq 3$ as an underlying theory of the electroweak symmetry breaking. (As an example of recent work on walking technicolor model based on $SU(2)$ gauge theory, see [46, 47].) So it is interesting to investigate \hat{S} and

α_*	$\Pi_{V-A}(Q^2 = 0)/\Lambda^2 = f_\pi^2/\Lambda^2$	$\Pi_{V-A}(Q^2 = f_\pi^2)/\Lambda^2$	\hat{S}_*
0.890	6.05×10^{-10}	5.90×10^{-10}	0.308
0.895	1.08×10^{-9}	1.05×10^{-9}	0.309
0.900	1.85×10^{-9}	1.80×10^{-9}	0.311
0.905	3.09×10^{-9}	3.01×10^{-9}	0.311
0.910	5.00×10^{-9}	4.88×10^{-9}	0.311
0.915	7.91×10^{-9}	7.71×10^{-9}	0.312
0.920	1.22×10^{-8}	1.19×10^{-8}	0.313
0.925	1.85×10^{-8}	1.80×10^{-8}	0.314
0.930	2.74×10^{-8}	2.67×10^{-8}	0.314
0.935	3.99×10^{-8}	3.89×10^{-8}	0.315
0.940	5.72×10^{-8}	5.57×10^{-8}	0.316
0.945	8.06×10^{-8}	7.86×10^{-8}	0.316
0.950	1.12×10^{-7}	1.09×10^{-7}	0.317
0.955	1.54×10^{-7}	1.50×10^{-7}	0.318
0.960	2.08×10^{-7}	2.03×10^{-7}	0.318
0.965	2.78×10^{-7}	2.71×10^{-7}	0.319
0.970	3.68×10^{-7}	3.59×10^{-7}	0.320
0.975	4.82×10^{-7}	4.70×10^{-7}	0.320
0.980	6.25×10^{-7}	6.09×10^{-7}	0.321
0.985	8.02×10^{-7}	7.82×10^{-7}	0.321
0.990	1.02×10^{-6}	9.96×10^{-7}	0.322
0.995	1.29×10^{-6}	1.26×10^{-6}	0.322
1.000	1.62×10^{-6}	1.57×10^{-6}	0.323

Table 2: Values of $\Pi_{V-A}(Q^2 = 0)/\Lambda^2 = f_\pi^2/\Lambda^2$, $\Pi_{V-A}(Q^2 = f_\pi^2)/\Lambda^2$, and \hat{S}_* for several values of α_* .

Δm_π^2 in the case of $N_c \neq 3$ in future works.

Acknowledgments

We would like to thank Robert Shrock for very illuminating discussions and criticism. We also thank Masaharu Tanabashi for useful discussions. This work was supported in part by the JSPS Grant-in-Aid for the Scientific Research (B)(2) 14340072, The Mitsubishi Foundation and by the 21st Century COE Program of Nagoya University provided by JSPS (15COEG01). This work was also supported in part by (C)(2) 16540241 (M.H.), the Daiko Foundation #9099 (M.H.), the MEXT Grant-in-Aid for Scientific Research No.14046201 (M.K.) and the grant NSF-PHY-00-98527 at YITP, SUNY Stony Brook (M.K.). M.K. acknowledges the hospitality of the Aspen Center for Physics where part of this work was done.

Appendices

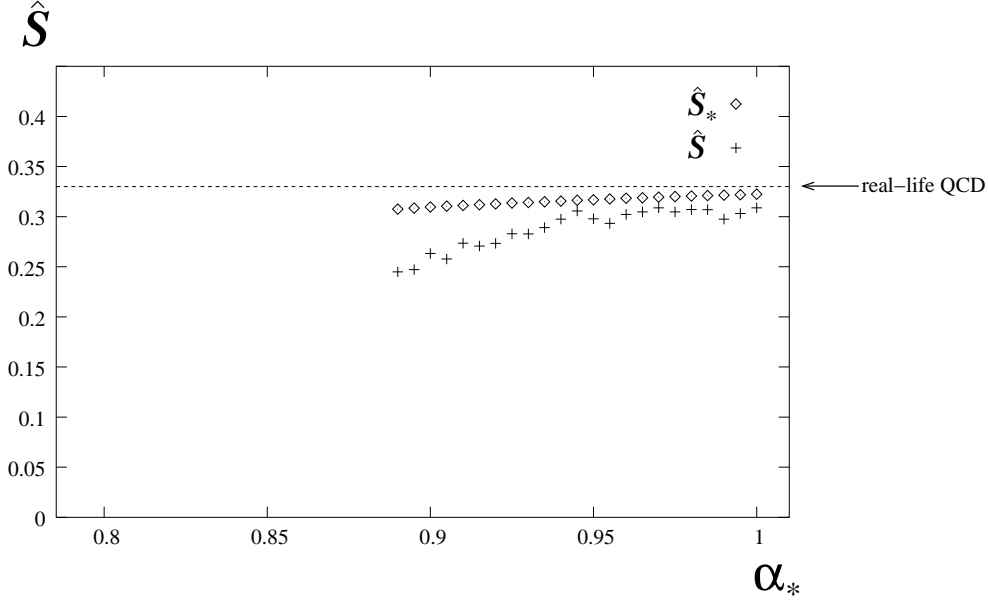


Figure 11: Values of \hat{S}_* shown in Table 2. Values of \hat{S} are also plotted in the figure.

$$iS_F^{-1}(p) - \not{p} = \text{[Diagram: A fermion line with momentum p and q, a shaded circle representing a full fermion propagator, and a wavy line representing a gauge boson propagator.]}$$

full fermion propagator

Figure 12: A graphical expression of the SD equation in the (improved) ladder approximation.

A Appendix : SD equation in the improved ladder approximation

Schwinger-Dyson (SD) equation is a powerful tool to study the dynamical generation of the fermion mass directly from QCD (for reviews, see, e.g., Refs. [22, 48]). The SD equation for the full fermion propagator $iS_F^{-1} = A(p^2)\not{p} - B(p^2)$ in the improved ladder approximation [35] is given by (see Fig. 12 for a graphical expression)

$$iS_F^{-1}(p) - \not{p} = C_2 \int \frac{d^4q}{i(2\pi)^4} \bar{g}^2(p, q) \frac{1}{(p-q)^2} \left(g_{\mu\nu} - \frac{(p-q)_\mu(p-q)_\nu}{(p-q)^2} \right) \gamma^\mu iS_F(q) \gamma^\nu, \quad (\text{A.1})$$

where $C_2 (= \frac{N_c^2-1}{2N_c})$ is the second casimir invariant, $\bar{g}(p, q)$ is the running coupling, and the Landau gauge is adopted for the gauge boson propagator. The SD equation provides coupled equations for two functions A and B in the full fermion propagator S_F . When we adopt a simple ansatz for the running coupling, $\bar{g}^2(p, q) = \bar{g}^2(\max(p_E^2, q_E^2))$ [35], with (p_E^2, q_E^2) being the Euclidean momenta, we can carry out

the angular integration and get $A(p^2) \equiv 1$ in the Landau gauge. Then the SD equation becomes a self-consistent equation for the mass function $\Sigma(p^2) \equiv B(p^2)$. The resultant asymptotic behavior of the dynamical mass $\Sigma(p^2)$ is shown to coincide with that obtained by the operator product expansion technique.

However, it was shown in Ref. [42] that the axial Ward-Takahashi identity is violated in the improved ladder approximation unless the gluon momentum is used as the argument of the running coupling as $\bar{g}^2((p_E - q_E)^2)$. In this choice we cannot carry out the angle integration analytically since the running coupling depends on the angle factor $\cos \theta = p_E \cdot q_E / |p_E||q_E|$. Furthermore, we would need to introduce a nonlocal gauge fixing [49, 42] to preserve the condition $A = 1$.

In Ref. [50], however, it was shown that an angle averaged form $\bar{g}^2(p_E^2 + q_E^2)$ gives a good approximation. Then, in the present analysis we take the argument of the running coupling as

$$\bar{g}^2(p_E, q_E) \Rightarrow \bar{g}^2(p_E^2 + q_E^2). \quad (\text{A.2})$$

After applying this angle average approximation and carrying out the angular integration, we can show (see, e.g., Refs. [48]) that A always satisfies $A(p^2) = 1$ in the Landau gauge. Then the SD equation becomes

$$\Sigma(x) = C_2 \frac{3}{16\pi^2} \int dy \frac{y \Sigma(y)}{y + \Sigma^2(y)} \frac{\bar{g}^2(x+y)}{\max(x, y)}, \quad (\text{A.3})$$

where $x = p_E^2$ and $y = q_E^2$.

B Appendix : Numerical method for solving the SD equation

In this appendix we briefly explain how to solve the SD equation numerically.

We first introduce the infrared (IR) cutoff λ_{SD} and ultraviolet (UV) cutoff Λ_{SD} as

$$\Lambda^2 e^{\lambda_{SD}/\Lambda} \leq x, y \leq \Lambda^2 e^{\Lambda_{SD}/\Lambda}. \quad (\text{B.1})$$

Then, we discretize the momentum variable x and y into N_{SD} points as

$$x_i = \Lambda^2 \exp \left[\lambda_{SD}/\Lambda + D_{SD} \cdot i \right], \quad (i = 0, 1, 2, \dots, (N_{SD} - 1)), \quad (\text{B.2})$$

where

$$D_{SD} = \frac{(\Lambda_{SD} - \lambda_{SD})/\Lambda}{N_{SD} - 1}. \quad (\text{B.3})$$

Accordingly, the integration over y is replaced with a summation as

$$\int dy \Rightarrow D_{SD} \sum_j y_j. \quad (\text{B.4})$$

Then, the SD equation in Eq. (A.3) with the running coupling in Eq. (A.2) is rewritten as

$$\Sigma(x_i) = \frac{1}{4\pi^2} D_{SD} \sum_j \bar{g}^2(x_i + y_j) \frac{y_j^2}{\max(x_i, y_j)} \frac{\Sigma(y_j)}{y_j + \Sigma^2(y_j)}. \quad (\text{B.5})$$

This discretized version of the SD equation is solved by the recursion relation:

$$\Sigma_{(n+1)}(x_i) = \frac{1}{4\pi^2} D_{SD} \sum_j \bar{g}^2(x_i + y_j) \frac{y_j^2}{\max(x_i, y_j)} \frac{\Sigma_{(n)}(y_j)}{y_j + \Sigma_{(n)}^2(y_j)}. \quad (\text{B.6})$$

Starting from a suitable initial condition (we choose $\Sigma_{(0)}(x_i) = 1$), we update the mass function by the above recursion relation. Then, we stop the iteration when the convergence condition

$$D_{SD} \sum_i \frac{x_i^2}{16\pi^2} \left[\Sigma_{(n+1)}(x_i) - \Sigma_{(n)}(x_i) \right]^2 < \varepsilon^2 \Lambda^6 \quad (\text{B.7})$$

is satisfied for sufficiently small ε , and regard this $\Sigma_{(n)}$ as a solution of Eq. (B.5).

In the present paper, we use the following parameters to solve the SD equation numerically:

$$\Lambda_{SD}/\Lambda = +24 \quad , \quad \lambda_{SD}/\Lambda = -24 \quad , \quad N_{SD} = 1000 \quad , \quad \varepsilon = 10^{-20}. \quad (\text{B.8})$$

C Appendix : Numerical method for solving the IBS equation

In this appendix we transform the IBS equation in Eq. (5.1) into the form in which we can solve it numerically.

First, we introduce the conjugate bispinor bases defined by

$$\bar{\Gamma}_i^{(J)}(p; q, \epsilon) \equiv \gamma_0 \Gamma_i^{(J)}(p^*; q, \epsilon)^\dagger \gamma_0. \quad (\text{C.1})$$

Multiplying these conjugate bispinor bases from left, taking the trace of spinor indices and summing over the polarizations, we rewrite Eq. (5.1) into the following form:

$$T_{ij}^{(J)}(u, x) \chi_j^{(J)}(u, x) - \frac{1}{8\pi^3} \int_{-\infty}^{\infty} dv \int_0^{\infty} dy y^2 K_{ij}^{(J)}(u, x; v, y) \chi_j^{(J)}(v, y) = I_i^{(J)}(u, x), \quad (\text{C.2})$$

where the summation over the index j is understood, and

$$I_i^{(J)} = \sum_{\epsilon} \text{tr} \left[\bar{\Gamma}_i^{(J)}(p; q, \epsilon) (\epsilon \cdot G^{(J)}) \right], \quad (\text{C.3})$$

$$T_{ij}^{(J)}(u, x) = \sum_{\epsilon} \text{tr} \left[\bar{\Gamma}_i^{(J)}(p; q, \epsilon) T(p; q) \Gamma_j^{(J)}(p; q, \epsilon) \right], \quad (\text{C.4})$$

$$K_{ij}^{(J)}(u, x; v, y) = \int_{-1}^1 d \cos \theta \sum_{\epsilon} \text{tr} \left[\bar{\Gamma}_i^{(J)}(p; q, \epsilon) K(p, k) \Gamma_j^{(J)}(k; q, \epsilon) \right], \quad (\text{C.5})$$

with the real variables v and y introduced as

$$k \cdot q = -v Q, \quad k \cdot p = -uv - xy \cos \theta. \quad (\text{C.6})$$

Here θ is the angle between the spatial components of p_{μ} and k_{μ} .

Using the property of $\chi_i^{(J)}$ in Eq. (4.10), we restrict the integration range as $v > 0$:

$$\int dv K_{ij}(u, x; v, y) \chi_j^{(J)}(v, y) = \int_{v>0} dv [K_{ij}(u, x; v, y) + K_{ij}(u, x; -v, y)] \chi_j^{(J)}(v, y). \quad (\text{C.7})$$

Then, in the following, we treat all the variables u, x, v and y as positive values.

To discretize the variables u, x, v and y we introduce new variables U, X, V and Y as

$$\begin{aligned} u &= e^U, & x &= e^X, \\ v &= e^V, & y &= e^Y, \end{aligned} \quad (\text{C.8})$$

and set ultraviolet (UV) and infrared (IR) cutoffs as

$$U, V \in [\lambda_U, \Lambda_U], \quad X, Y \in [\lambda_X, \Lambda_X]. \quad (\text{C.9})$$

We discretize the variables U and V into $N_{BS,U}$ points evenly, and X and Y into $N_{BS,X}$ points. Then, the original variables are labeled as

$$\begin{aligned} u_{[I_U]} &= \exp[\lambda_U + D_U I_U], & x_{[I_X]} &= \exp[\lambda_X + D_X I_X], \\ v_{[I_V]} &= \exp[\lambda_U + D_U I_V], & y_{[I_Y]} &= \exp[\lambda_X + D_X I_Y], \end{aligned}$$

where $I_U, I_V = 0, 1, 2, \dots, (N_{BS,U} - 1)$ and $I_X, I_Y = 0, 1, 2, \dots, (N_{BS,X} - 1)$. The measures D_U and D_X are defined as

$$D_U = \frac{\Lambda_U - \lambda_U}{N_{BS,U} - 1}, \quad D_X = \frac{\Lambda_X - \lambda_X}{N_{BS,X} - 1}. \quad (\text{C.10})$$

As a result, the integration is converted into the summation:

$$\int_{v>0} y^2 dy dv \dots \implies D_U D_V \sum_{I_V, I_Y} v y^3 \dots \quad (\text{C.11})$$

In order to avoid integrable singularities in the kernel $K(u, x; v, y)$ at $(u, x) = (v, y)$, we adopt the following four-splitting prescription [51]:

$$\begin{aligned} K_{ij}(u, x, v, y) \implies & \frac{1}{4} [K_{ij}(u, x, v_+, y_+) + K_{ij}(u, x, v_+, y_-) \\ & + K_{ij}(u, x, v_-, y_+) + K_{ij}(u, x, v_-, y_-)], \end{aligned} \quad (\text{C.12})$$

where

$$v_{\pm} = \exp\left[V \pm \frac{D_U}{4}\right], \quad y_{\pm} = \exp\left[Y \pm \frac{D_X}{4}\right]. \quad (\text{C.13})$$

Now that all the variables have become discrete and the original integral equation (5.1) has turned into a linear algebraic one, we are able to deal it numerically.

When we solve the IBS equation numerically in this paper, we use the following parameters :

$$\begin{aligned} [\lambda_U, \Lambda_U] &= [34.5 \times \alpha_* - 45.0, \quad 0.0], \\ [\lambda_X, \Lambda_X] &= [43.5 \times \alpha_* - 52.0, \quad 0.0], \\ N_{BS,U} &= N_{BS,X} = 34. \end{aligned} \quad (\text{C.14})$$

Note that $[\lambda_U, \Lambda_U]$ and $[\lambda_X, \Lambda_X]$ are chosen so that the dominant supports of $\Pi_{VV}(Q^2) - \Pi_{AA}(Q^2)$ always lie within the energy region between UV and IR cutoffs.

References

- [1] M. Harada, M. Kurachi and K. Yamawaki, in *Proc. of 2004 International Workshop on Dynamical Symmetry Breaking, Nagoya, Japan, 21-22 Dec 2004*, ed. M. Harada and K. Yamawaki, (Nagoya University, 2005) pp. 125-140.
- [2] T. Banks and A. Zaks, Nucl. Phys. B **196**, 189 (1982).
- [3] T. Appelquist, J. Terning and L. C. Wijewardhana, Phys. Rev. Lett. **77**, 1214 (1996); T. Appelquist, A. Ratnaweera, J. Terning and L. C. Wijewardhana, Phys. Rev. D **58**, 105017 (1998).
- [4] V. A. Miransky and K. Yamawaki, Phys. Rev. D **55**, 5051 (1997) [Erratum-ibid. D **56**, 3768 (1997)].
- [5] Y. Iwasaki, K. Kanaya, S. Sakai and T. Yoshie, Phys. Rev. Lett. **69**, 21 (1992); Y. Iwasaki, K. Kanaya, S. Kaya, S. Sakai and T. Yoshie, Nucl. Phys. Proc. Suppl. **53**, 449 (1997); Prog. Theor. Phys. Suppl. **131**, 415 (1998). See also J. B. Kogut and D. K. Sinclair, Nucl. Phys. B **295**, 465 (1988); F. R. Brown, H. Chen, N. H. Christ, Z. Dong, R. D. Mawhinney, W. Schaffer and A. Vaccarino, Phys. Rev. D **46**, 5655 (1992).
- [6] R. Oehme and W. Zimmermann, Phys. Rev. D **21**, 471 (1980).
- [7] M. Velkovsky and E. Shuryak, Phys. Lett. B **437**, 398 (1998).
- [8] M. Harada and K. Yamawaki, Phys. Rev. Lett. **83**, 3374 (1999).
- [9] M. Harada and K. Yamawaki, Phys. Rev. Lett. **86**, 757 (2001); Phys. Rept. **381**, 1 (2003)
- [10] H. Gies and J. Jaeckel, arXiv:hep-ph/0507171.
- [11] S. Weinberg, Phys. Rev. D **13**, 974 (1976); Phys. Rev. D **19**, 1277 (1979); L. Susskind, Phys. Rev. D **20**, 2619 (1979).
- [12] See for reviews, e.g., E. Farhi and L. Susskind, Phys. Rept. **74**, 277 (1981); C. T. Hill and E. H. Simmons, Phys. Rept. **381**, 235 (2003) [Erratum-ibid. **390**, 553 (2004)] and references therein.
- [13] K. Yamawaki, M. Bando and K. Matumoto, Phys. Rev. Lett. **56**, 1335 (1986); T. Akiba and T. Yanagida, Phys. Lett. B **169**, 432 (1986); T.W. Appelquist, D. Karabali and L.C.R. Wijewardhana, Phys. Rev. Lett. **57**, 957 (1986); M. Bando, T. Morozumi, H. So and K. Yamawaki, Phys. Rev. Lett. **59**, 389 (1987); See also B. Holdom, Phys. Lett. B **150**, 301 (1985).
- [14] F. N. Ndili, arXiv:hep-ph/0508111.
- [15] V. A. Kuzmin, V. A. Rubakov and M. E. Shaposhnikov, Phys. Lett. B **155**, 36 (1985).

- [16] A. G. Cohen, D. B. Kaplan and A. E. Nelson, *Ann. Rev. Nucl. Part. Sci.* **43**, 27 (1993) [arXiv:hep-ph/9302210].
- [17] R. D. Pisarski and F. Wilczek, *Phys. Rev. D* **29**, 338 (1984).
- [18] A. Martin and K. Lane, *Phys. Rev. D* **71**, 015011 (2005) [arXiv:hep-ph/0404107].
- [19] R. S. Chivukula, *Phys. Rev. D* **55**, 5238 (1997).
- [20] M. Bando, T. Kugo, S. Uehara, K. Yamawaki and T. Yanagida, *Phys. Rev. Lett.* **54**, 1215 (1985) ; M. Bando, T. Kugo and K. Yamawaki, *Nucl. Phys. B* **259**, 493 (1985); *Prog. Theor. Phys.* **73**, 1541 (1985); *Phys. Rept.* **164**, 217 (1988).
- [21] M. Harada, M. Kurachi and K. Yamawaki, *Phys. Rev. D* **68**, 076001 (2003)
- [22] T. Kugo, *in Proc. of 1991 Nagoya Spring School on Dynamical Symmetry Breaking, Nakatsugawa, Japan, Apr 23-27, 1991* ed. K. Yamawaki (World Scientific Pub. Co., 1992) pp.35-70.
- [23] M. Harada, M. Kurachi and K. Yamawaki, *Phys. Rev. D* **70**, 033009 (2004).
- [24] N. Arkani-Hamed, A. G. Cohen and H. Georgi, *Phys. Lett. B* **513**, 232 (2001)
N. Arkani-Hamed, A. G. Cohen, E. Katz, A. E. Nelson, T. Gregoire and J. G. Wacker, *JHEP* **0208**, 021 (2002) N. Arkani-Hamed, A. G. Cohen, E. Katz and A. E. Nelson, *JHEP* **0207**, 034 (2002)
- [25] C. Csaki, C. Grojean, H. Murayama, L. Pilo and J. Terning, *Phys. Rev. D* **69**, 055006 (2004); C. Csaki, C. Grojean, L. Pilo and J. Terning, *Phys. Rev. Lett.* **92**, 101802 (2004) ; Y. Nomura, *JHEP* **0311**, 050 (2003) ; R. Barbieri, A. Pomarol and R. Rattazzi, *Phys. Lett. B* **591**, 141 (2004) ; C. Csaki, C. Grojean, J. Hubisz, Y. Shirman and J. Terning, *Phys. Rev. D* **70**, 015012 (2004); H. Davoudiasl, J. L. Hewett, B. Lillie and T. G. Rizzo, *Phys. Rev. D* **70**, 015006 (2004); G. Burdman and Y. Nomura, *Phys. Rev. D* **69**, 115013 (2004); G. Cacciapaglia, C. Csaki, C. Grojean and J. Terning, *Phys. Rev. D* **70**, 075014 (2004).
- [26] M. E. Peskin and T. Takeuchi, *Phys. Rev. Lett.* **65**, 964 (1990); *Phys. Rev. D* **46**, 381 (1992); B. Holdom and J. Terning, *Phys. Lett. B* **247**, 88 (1990); M. Golden and L. Randall, *Nucl. Phys. B* **361**, 3 (1991).
- [27] R. Sundrum and S. D. H. Hsu, *Nucl. Phys. B* **391**, 127 (1993) ;T. Appelquist and G. Triantaphyllou, *Phys. Lett. B* **278**, 345 (1992).
- [28] T. Appelquist and F. Sannino, *Phys. Rev. D* **59**, 067702 (1999).
- [29] T. Takeuchi, *in Perspectives of Strong Coupling Gauge Theories*, Proceedings of the International Workshop, Nagoya, Japan, 1996, edited by J. Nishimura and K. Yamawaki (World Scientific, Singapore, 1997), pp. 150-155.
- [30] M. Harada, M. Tanabashi and K. Yamawaki, *Phys. Lett. B* **568**, 103 (2003).

- [31] B. Holdom, Phys. Lett. B **198**, 535 (1987).
- [32] M. Harada and Y. Yoshida, Phys. Rev. D **50**, 6902 (1994)
- [33] E. Gardi and M. Karliner, Nucl. Phys. B **529**, 383 (1998); E. Gardi, G. Grunberg and M. Karliner, JHEP **9807**, 007 (1998).
- [34] R. M. Corless, G. H. Gonnet, D. G. E. Hare, D. J. Jeffrey and D. E. Knuth, Adv. Comput. Math. **5**, 329 (1996).
- [35] V. A. Miransky, Sov. J. Nucl. Phys. **38**, 280 (1983) [Yad. Fiz. **38**, 468 (1983)]; K. Higashijima, Phys. Rev. D **29**, 1228 (1984).
- [36] S. Weinberg, Phys. Rev. Lett. **18**, 507 (1967).
- [37] S. Eidelman *et al.* [Particle Data Group Collaboration], Phys. Lett. B **592**, 1 (2004), and 2005 partial update for edition 2006 (URL: <http://pdg.lbl.gov>).
- [38] T. Das, V. S. Mathur and S. Okubo, Phys. Rev. Lett. **19**, 859 (1967).
- [39] K. Yamawaki, Phys. Lett. B **118**, 145 (1982).
- [40] T. Das, G. S. Guralnik, V. S. Mathur, F. E. Low and J. E. Young, Phys. Rev. Lett. **18**, 759 (1967)
- [41] M.E. Peskin, Nucl. Phys. B **175**, 197 (1980); J. Preskill, Nucl. Phys. B **177**, 21 (1981).
- [42] T. Kugo and M. G. Mitchard, Phys. Lett. B **282**, 162 (1992); Phys. Lett. B **286**, 355 (1992).
- [43] M. Bando, M. Harada and T. Kugo, Prog. Theor. Phys. **91**, 927 (1994).
- [44] M. A. Shifman, A. I. Vainshtein and V. I. Zakharov, Nucl. Phys. B **147**, 385 (1979); Nucl. Phys. B **147**, 448 (1979).
- [45] A. G. Cohen and H. Georgi, Nucl. Phys. B **314**, 7 (1989).
- [46] D. D. Dietrich, F. Sannino and K. Tuominen, Phys. Rev. D **72**, 055001 (2005) [arXiv:hep-ph/0505059].
- [47] N. D. Christensen and R. Shrock, arXiv:hep-ph/0509109.
- [48] V. A. Miransky, “Dynamical symmetry breaking in quantum field theories,” *Singapore, Singapore: World Scientific (1993) 533 p.*
- [49] H. Georgi, E. H. Simmons and A. G. Cohen, Phys. Lett. B **236**, 183 (1990).
- [50] K. I. Aoki, M. Bando, T. Kugo and M. G. Mitchard, Prog. Theor. Phys. **85**, 355 (1991).
- [51] K. I. Aoki, T. Kugo and M. G. Mitchard, Phys. Lett. B **266**, 467 (1991).